DISSERTATIONES CHIMICAE UNIVERSITATIS TARTUENSIS
112

DISSERTATIONES CHIMICAE UNIVERSITATIS TARTUENSIS
112

HEISI KURIG

Electrical double-layer capacitors based on ionic liquids as electrolytes

TARTU UNIVERSITY PRESS

Institute of Chemistry, Faculty of Science and Technology, University of Tartu, Estonia

Dissertation is accepted for the commencement of the degree of Doctor of Philosophy in Chemistry on 24th October, 2011 by the Council of Institute of Chemistry, University of Tartu.

Supervisors:	Prof. Enn Lust, University of Tartu, Estonia
	Dr. Alar Jänes, University of Tartu, Estonia
Opponent:	Prof. François Béguin, University of Orléans, France
Commencement:	December 20th, 2011, 10:00

European Union
European Social Fund

Investing in your future

ISSN 1406–0299
ISBN 978–9949–19–908–2 (trükis)
ISBN 978–9949–19–909–9 (PDF)

Tartu Ülikooli Kirjastus
www.tyk.ee
Tellimus nr. 740

TABLE OF CONTENTS

1. LIST OF ORIGINAL PUBLICATIONS 7

2. ABBREVIATIONS AND SYMBOLS 8

3. INTRODUCTION 10

4. LITERATURE OVERVIEW AND INTERPRETATION OF DATA 11
   - 4.1. Electrical double-layer capacitors 11
     - 4.1.1. Electrical double-layer theories 12
     - 4.1.2. Carbon as electrode material in EDLCs 13
     - 4.1.3. Gas adsorption theories for carbon characterization 15
       - 4.1.3.1. The Brunauer-Emmett-Teller theory 15
       - 4.1.3.2. t-plot method 16
       - 4.1.3.3. Total pore volume 17
       - 4.1.3.4. Non-local density functional theory 17
     - 4.1.4. Separators in EDLCs 18
     - 4.1.5. Electrolytes in EDLCs 18
   - 4.2. Room-temperature ionic liquids 19
     - 4.2.1. Influence of temperature to the electrical conductivity of ionic liquids 19
     - 4.2.2. Electrochemical stability of RTILs 20
   - 4.3. COSMOtherm calculations 21
   - 4.4. Electrochemical measurement techniques and interpretation of data 22
     - 4.4.1. Cyclic voltammetry 22
     - 4.4.2. Electrochemical impedance spectroscopy 23
     - 4.4.3. Calculation of complex power and characteristic relaxation time constant 26
     - 4.4.4. Modelling the electrochemical impedance data with equivalent circuit 30

5. EXPERIMENTAL 32
   - 5.1. Electrode materials and preparation of electrodes 32
   - 5.2. Characteristics of ionic liquids 32
   - 5.3. Melting point, conductivity and viscosity measurements 33
   - 5.4. Assembling EDLC test-cells and electrochemical measurements 34

6. RESULTS AND DISCUSSION 35
   - 6.1. The electrochemical behavior of different RTIL based EDLCtcs at room-temperature 35
     - 6.1.1. Cyclic voltammetry data and analysis for different RTIL based EDLCtcs 35
     - 6.1.2. Electrochemical impedance spectroscopy data and analysis for different RTIL based EDLCtcs 39
     - 6.1.3. Modelling the electrochemical impedance spectroscopy data 42
   - 6.2. Influence of temperature on $EMImBF_4$ based EDLCtc electrochemical behavior and physical properties 46

6.2.1. Influence of temperature on conductivity and viscosity of bulk $EMImBF_4$ 46
6.2.2. Cyclic voltammetry data and analysis for EMImBF4 based EDLCtcs at different temperatures 47
6.2.3. Electrochemical impedance spectroscopy data and analysis for $EMImBF_4$ based EDLCtcs at different temperatures 48
6.3. Comparison of RTILs and other electrolytes in EDLCtcs 52
7. SUMMARY 57
8. REFERENCES 58
9. SUMMARY IN ESTONIAN 62
10. ACKNOWLEDGEMENTS 63
11. PUBLICATIONS 65

1. LIST OF ORIGINAL PUBLICATIONS

I. H. Kurig, A. Jänes, E. Lust, Electrochemical characteristics of carbide-derived carbon|1-ethyl-3-methylimidazolium tetrafluoroborate supercapacitor cells, J. Electrochem. Soc. 157 (2010) A272–A279.

II. H. Kurig, A. Jänes, E. Lust, Substituted phosphonium cation based electrolytes for nonaqueous electrical double-layer capacitors, J. Mater. Res. 25 (2010) 1447–1450.

III. A. Jänes, H. Kurig, T. Romann, E. Lust, Novel doubly charged cation based electrolytes for non-aqueous supercapacitors, Electrochem. Commun. 12 (2010) 535–539.

IV. H. Kurig, T. Romann, A. Jänes, E. Lust, Electrochemical characteristics of titanium carbide derived carbon|1-ethyl-3-methylimidazolium tetrafluoroborate electrical double layer capacitors, ECS Trans. 25 (2010) 15–23.

V. H. Kurig, M. Vestli, A. Jänes, E. Lust, Electrical double layer capacitors based on two 1-ethyl-3-methylimidazolium ionic liquids with different anions, Electrochem. Solid-State Lett. 14 (2011) A120-A122.

VI. H. Kurig, M Vestli, K. Tõnurist, A. Jänes, E. Lust, Electrochemical behavior and physical properties of 1-ethyl-3-methylimidazolium cation and different anion based ionic liquids with perspective as supercapacitor electrolyte (under review).

Author's contribution

Paper I: Performed all electrochemical measurements and analysis of data. Participated in preparation of the manuscript.

Paper II: Performed all electrochemical measurements and analysis of data. Mainly responsible for the preparation of manuscript.

Paper III: Performed all electrochemical measurements. Participated in the analysis of data and preparation of the manuscript.

Paper IV: Performed all electrochemical measurements and analysis of data. Mainly responsible for the preparation of manuscript.

Paper V: Performed all electrochemical measurements and analysis of data. Mainly responsible for the preparation of manuscript.

Paper VI: Performed all electrochemical measurements and analysis of data. Mainly responsible for the preparation of manuscript.

2. ABBREVIATIONS AND SYMBOLS

A_{cs}	cross-section area of adsorbate
AN	acetonitrile
BET theory	Brunauer-Emmett-Teller theory
C	total capacitance
c	constant in BET theory
C'	real part of the capacitance
C''	imaginary part of the capacitance
C_{ads}	capacitance corresponding to the adsorption process
C_{CV}	capacitance of one electrode calculated from cyclic voltammetry data
C_D	capacitance of diffuse layer
C_{ef}	"true" interfacial capacitance without adsorption effects calculated at high frequencies
C_H	Helmholtz capacitance of Stern layer
CPE	constant phase element
C_s	series capacitance of one electrode
D	diffusion coefficient
d	pore width
D_{eff}	effective diffusion coefficient of ions
DMC	dimethyl carbonate
EC	ethylene carbonate
EDLC	electrical double-layer capacitor
EDLCtc	electrical double-layer capacitor test-cell
E	electrode potential
E_{max}	maximal specific energy
f	alternative current frequency
f_0	characteristic relaxation frequency
$f(d)$	function of pore size distribution
I_{CV}	current density in cyclic voltammograms
L_{eff}	effective diffuse layer thickness
L_{eff}^2 / D_{eff}	so-called mass-transfer frequency parameter
M	molecular mass
m_{am}	active mass of one electrode
n	number of electrons transferred in the electrochemical reaction
$N(P/P_0)$	point in NLDFT adsorption isotherm
$N(P/P_0,d)$	point in NLDFT adsorption isotherm corresponding to the pore with width d
NLDFT	non-local density functional theory
Ox	oxidant
P	pressure
P_0	atmospheric pressure
P/P_0	relative pressure

PC	propylene carbonate
P_{max}	maximal specific power
$P(\omega)$	active power (i.e. real) component of complex power
Q_1	heat of adsorption for first layer
Q_{liq}	heat of adsorption for second and higher layers, heat of liquefaction
$Q(\omega)$	reactive (i.e. imaginary) power component of complex power
R	total resistance
$\overline{R}$	ideal gas constant
R_{ads}	adsorption resistance
Red	reducer
R_{el}	total high frequency series resistance
R_D	resistance of diffusion-like processes
R_p	parallel resistance
R_{PHF}	high frequency polarization resistance
R_s	series resistance
RTIL	room-temperature ionic liquid
$S(\omega)$	complex power
T	temperature
t	time
T_g	glass transition temperature
t_{stat}	statistical thickness of adsorbed layer
U	test-cell voltage
V_{ads}	volume of adsorbed gas
V_{molar}	the molar volume of adsorbate
V_t	total pore volume
WAPS	weighted average positive charge density
W	mass of gas adsorbed
W_m	mass of gas in monolayer
Z	impedance
Z'	real part of impedance
Z''	imaginary part of impedance
Z_{GFW}	generalized finite Warburg element
α_W	Warburg fractional exponent
γ-BL	γ-butyrolactone
η	dynamic viscosity
κ	specific conductivity
ν	potential or voltage scan rate
θ	phase angle between voltage and current
σ	charge density
τ_0	characteristic relaxation time
τ_D	diffusion relaxation time
ω	angular frequency

3. INTRODUCTION

Electrical double-layer capacitors (EDLCs), also known as supercapacitors and ultracapacitors, are modern energy storage devices with short charging and discharging times and power and energy stored per volume or mass in EDLCs is orders larger compared to conventional dielectrical capacitors [1–5]. So far, the best energy density, power densities and cyclability have been established for EDLCs with acetonitrile (AN) or organic carbonate based electrolytes [2, 4, 5, 7–10]. Unfortunately, the toxicity of AN, and the moderate vapor pressure of organic esters makes the replacement of organic solvents an important question for commercialization of safe and energetically effective EDLCs. One possibility is to use room-temperature ionic liquids (RTILs) as electrolytes for EDLC [11–30].

Selection of ionic liquids is very wide [11, 12, 31] and choosing suitable RTIL for EDLC application is a complex problem. The effects of chemical composition, structural properties and purity of RTILs on conductivity, viscosity and electrochemical stability of electrolyte, capacitance, energy and power density of EDLC etc. must be considered. To study the influence of chemical composition and structure of anion in RTIL to EDLC test-cell (EDLCtc) behavior, six ionic liquids consisting of 1-ethyl-3-methylimidazolium cation ($EMIm^+$) and tetrafluoroborate (BF_4^-), tetracyanoborate ($B(CN)_4^-$), tris(pentafluoroethyl)trisfluorophosphate ($PF_3(C_2F_5)_3^-$), bis(trifluoromethylsulfonyl)imide ($N(SO_2CF_3)_2^-$), bis(fluorosulfonyl)imide ($N(SO_2F)_2^-$) or thiocyanate (SCN^-) anion have been studied as electrolytes for EDLCs. Differences arising in electrochemical behavior have been compared to the trends in the conductivity, viscosity and charge delocalization of anion in bulk RTILs.

Although, it is well-known that the main disadvantage of ionic liquids as electrolytes is their relatively low conductivity and thus low power density of EDLCs based on RTILs. Some papers published by different authors suggest that RTIL based EDLCs should be used at elevated temperatures (for example at 60 °C) [15, 17, 18, 21–26] because increase in temperature increases the conductivity of bulk RTIL. However, it is questionable if the relations between bulk properties of ionic liquid and the properties of ionic liquid as electrolyte in electrolyte|electrode interface, porous electrode and separator matrix are so simple. Thus, the influence of temperature on electrochemical behavior of $EMImBF_4$ based EDLCtc has also been evaluated and explained.

Finally, to demonstrate the position of RTIL based EDLCtcs amongst organic solvent electrolyte based EDLCtcs, the results obtained for different RTILs are compared to other electrolytes studied by author.

4. LITERATURE OVERVIEW AND INTERPRETATION OF DATA

4.1. Electrical double-layer capacitors

In EDLCs the charge is accumulated in the electrical double-layer at the electrode|electrolyte interface. Because of the high surface area and the small thinness of the double-layer (0.5 to 1 nm), these devices can have very high specific and volumetric capacitances. Contrary to batteries, the charge in EDLCs is stored through non-faradaic processes and there is no electron transfer (faradaic processes) through the electrode|electrolyte interface. The charge is mainly stored through physical adsorption processes and thus the positive and negative ionic charges accumulate at the surface of the solid electrode and are compensated by the electronic charge at the electrode surface layer. This enables them to have very high power and energy densities for capacitors and high degree of recyclability, on the order of 10^5 – 10^6 times [1, 2, 4, 32–34]. The operational voltage is usually below 1 V or 3 V per cell, for aqueous or organic solvent based electrolytes, respectively [1, 2, 4–6].

Figure 1 shows a schematic diagram of an EDLCtc consisting of a high surface area electrode material, which is loaded with electrolyte. The electrodes are separated by porous separator, containing the same electrolyte as the active material.

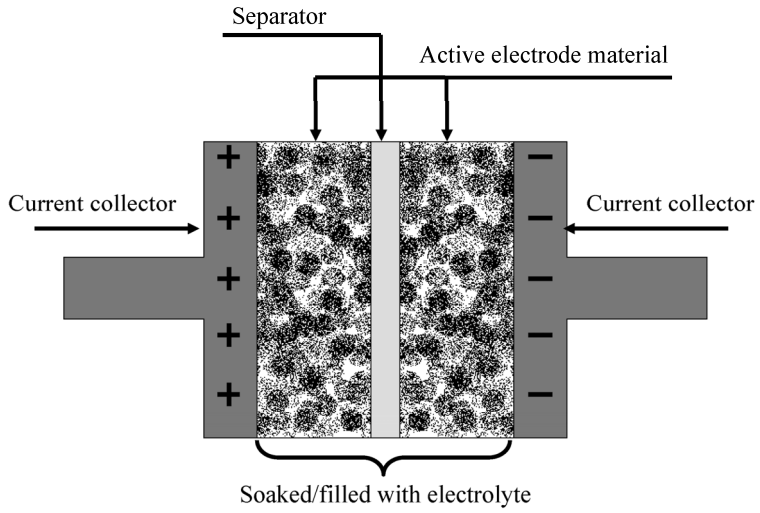

Figure 1. Principle of an electrical double-layer capacitor test-cell.

4.1.1. Electrical double-layer theories

The formation of new interphase is usually associated to a rearrangement of charges inside the phase and on the surface of electrode. This phenomenon is called the formation of electrical double-layer. Charges can be rearranged

(i) with direct charge transfer;
(ii) when ions with different charges have different surface activity;
(iii) when polarizable atoms and molecules are adsorbed and polarized on the interphase;
(iv) when molecules with permanent dipole moment are adsorbed and oriented on the interphase.

First electrical double-layer theory was proposed by H. Helmholtz in 1853 [35]. Helmholtz claimed that electrical double-layer consists of two parallel layers of counter charges. In the first approximation, the distance between these two layers is the diameter of charged particles and the charge in these layers is distributed uniformly all over the interphase. In Helmholtz theory the electrical double-layer can be treated as usual planar capacitor with differential capacitance, C,

$$C = \frac{\varepsilon\varepsilon_0}{l} \tag{1}$$

where ε_0 is the dielectrical permittivity for vacuum, ε is the relative dielectrical permittivity of environment and l is the distance between capacitor plates.

Helmholtz theory is in a reasonable accordance with experimental data, but it does not describe the dependence of differential capacitance and charge density on the temperature, electrolyte concentration and concentration of surface active additives in electrolyte etc. [36, 37].

The next model of electrical double-layer was developed independently by two scientist L. G. Gouy in 1910 [38] and D. L. Chapman in 1913 [39]. This diffuse layer model describes ions in solution as mathematical dots in constant heat motion. There is no compact Helmholtz layer on the interface [35, 37]. The Gouy-Chapman theory does not take into account the interactions between charged ions and ignores dimensions of ions being applicable only in dilute solutions.

The Helmholtz and Gouy-Chapman theory were integrated by O. Stern [40] who divided the electrical double-layer into two regions: *(i)* Helmholtz layer and *(ii)* diffuse layer where ions are in heat motion. The total charge of Helmholtz and diffuse layers is the opposite charge of the electronic charge at electrode surface [37, 41–44, 46].

These theories were elaborated by A. N. Frumkin and D. C. Grahame [42–45]. Grahame divided the Helmholtz layer into two components: *(i)* specifically adsorbed ions in Helmholtz inner plane and *(ii)* outer Helmholtz plane (without specific adsorption of ions). The outer Helmholtz plane is notional boundary with no energetic barrier between ions in heat motion in diffuse layer and ions

on interphase. The region between inner and outer Helmholtz plane is also known as Stern layer. In the case of no specific adsorption the electrical double-layer can be modelled as two capacitors connected in series [42, 43, 45]:

$$\frac{1}{C} = \frac{1}{C_{\mathrm{H}}} + \frac{1}{C_{\mathrm{D}}} \tag{2}$$

where C is the differential capacitance of electrical double-layer, C_{H} is the Helmholtz layer capacitance layer and C_{D} is the capacitance of diffuse layer.

There are also more complex theories like Rice, Fermi, modified Fermi, Hurwitz-Parsons etc. theories, which take into account the non-ideality of electrode surface properties, i.e. the potential drop inside the electrode surface layer or the specific adsorption effects of ions at electrode surface and additional interactions [41, 44, 46, 47].

4.1.2. Carbon as electrode material in EDLCs

Attraction of carbon as a EDLC electrode material arises from a unique combination of chemical and physical properties like high conductivity, high surface area (up to 2500 $m^2\ g^{-1}$), good corrosion resistance, high temperature stability, controlled pore structure, processability, compatibility in composite materials and relatively low cost [1–3, 5, 6, 34, 48]. In general, the first two properties have very strong influence on the EDLC electrochemical behavior.

The electrical properties of carbon particles are directly related to their structure. Increasing the ration of carbon in sp^2 hybridization state increases the conductivity inside the carbon particle (intra-resistance). However, the electrical resistance of a carbon electrode depends on intra-particle resistance and on the contact (inter-particle) resistance, i.e. the conductivity inside carbon particle and between different carbon particles in electrode layer determines the conductive properties of carbon electrode [3].

It is sometimes presumed that the capacitance of a porous carbon will be proportional to the surface area [49, 50]. Whilst sometimes this relationship can be observed, but in practice it usually represents an oversimplification [3, 5, 34]. The major factors that contribute to a complex non-linear relationship are *(i)* assumptions in the measurement of electrode surface area; *(ii)* variations in the specific capacitance of carbons with different material morphology; *(iii)* variations in surface chemistry; *(iv)* variations in the conditions under which capacitance for carbon electrode is measured. The surface areas of porous carbons and electrodes are most commonly measured by gas adsorption method (N_2 at 77 K) and surface area is estimated by applying Brunauer-Emmett-Teller (BET) theory [5, 51] (summarized later) to isotherm measured. Possibly the greatest constraint in attempting to correlate electrode differential capacitance with BET surface area, is the assumption that the surface accessed by nitrogen molecules is similar to the surface accessed by the electrolyte during the mea-

surement of differential capacitance. In addition, the wettability and pseudo-capacitive contributions of carbon electrode have not been considered in surface area estimation by gas sorption method [3].

There are many different carbon allotropic modifications and macroscopic forms that can be used as active materials in EDLC electrodes. Some of the most important carbon materials for EDLC electrodes are shortly reviewed below.

Activated carbon powders and fabrics. – Activated carbons are the most widely used active electrode materials for EDLC applications, because of their high surface area and relatively low cost. Activated carbon powders are derived from carbon-rich organic precursors (e.g. coconut shells, wood, pitch, coke, some synthetic polymers) by heat treatment in inert atmosphere. Activated carbon fabrics are produced from organic materials such as cellulose, phenolic resins, pitch-based materials, polyacrylonitrile and synthetic polymer materials. As compared to powders, activated carbon fabrics do not require any binder addition and can be directly used as active material films [3]. However, the cost of these carbon materials is higher compared to activated carbon powders [34].

High surface area of activated carbons is achieved through activation process consisting in a partial, controlled oxidation of the carbon precursor grains or fibers leading to development of porous network in the bulk of the carbon particles. Unfortunately, the pore size distribution in most activated carbons is not optimum because of poor pore size control in the activation process i.e. the high surface area of the carbon cannot be fully exploited to form the electrical double-layer [3, 5].

Carbide derived carbons. – Carbide derived carbons are derived from carbides via chlorination (or halogenation) reaction:

$$X_aC_y + \frac{az}{2}Cl_2 \rightarrow aXCl_z + yC$$

where, X is the carbide forming element in carbide (Si, Ti, Mo, V, W etc.). The micro- and macrostructure of carbide derived carbon is determined by the shape and structure of precursor carbide, synthesis temperature, selection and addition of catalyst making the properties (specific surface area, porosity, density etc.) of carbide derived carbon easily controllable. Carbide derived carbon electrode based EDLC demonstrate high specific capacitance (up to ~135 F g^{-1}) but, unfortunately, are much more expensive compared to activated carbon powders and fibers produced from organic material [5, 48, 52, 53].

Carbon nanostructures. – Carbon nanotubes and nanofibers are produced by the catalytic decomposition of certain hydrocarbons. By careful manipulation of various synthesis parameters, it is possible to generate nanostructures in assorted conformations and also control their crystalline order [3, 34, 54–57].

The specific capacitance of carbon nanotubes has been shown to be highly dependent on their morphology and purity. For purified nanotubes (i.e. without residual catalyst or amorphous carbon), the specific capacitance varies typically

from 15 to 80 F g^{-1} with surface areas that range from ~120 to 400 m^2 g^{-1} [3, 34, 52, 55]. The low specific capacitance values can somewhat be increased by oxidizing nanotubes, which modifies the surface structure of the carbon nanotubes and introduces or modifies surface functionalities to have some additional capacitance, so-called pseudocapacitance [3, 34, 52, 55–57].

Carbon aerogels. – Carbon aerogels are prepared by pyrolyzing organic aerogels synthesized by the polycondensation of resorchinol and formaldehyde with sol-gel method [3, 34]. A pyrolysis treatment in an inert atmosphere leads to the formation of a porous carbon aerogel with a controlled and uniform porous structure. Due to this ordered and interconnected pore structure, power capabilities of carbon aerogel based electrodes are generally high [3]. However, specific gravimetric capacitance values are rather moderate.

4.1.3. Gas adsorption theories for carbon characterization

According to IUPAC definition, the pores in solid materials are divided into three groups:

(i) pores with widths exceeding about 50 nm are called macropores;
(ii) pores of widths between 2 nm and 50 nm are called mesopores;
(iii) pores with widths not exceeding about 2 nm are called micropores.

Micropores are also known as nanopores as this name is in much better accordance with their actual size [4, 10, 48, 52].

4.1.3.1. The Brunauer-Emmett-Teller theory

The Brunauer-Emmett-Teller theory [51] is widely used to determine the specific surface area of materials according to following Equation (3):

$$\frac{1}{W((P/P_0)-1)} = \frac{1}{W_m c} + \frac{c-1}{W_m c}\left(\frac{P}{P_0}\right) \tag{3}$$

where W is the mass of gas adsorbed at relative pressure P/P_0, W_m is the mass of gas in monolayer and c is the constant in BET theory. Constant c describes the interactions between adsorbent and adsorbate and is expressed by Equation (4):

$$c = \exp\left(\frac{Q_1 - Q_{liq}}{\overline{R}T}\right) \tag{4}$$

where, $\overline{R}$ is ideal gas constant, T is temperature, Q_1 is heat of adsoption for the first adsorbate layer and Q_{liq} is heat of adsorption for second and higher layers and is equal to the heat of liquefaction.

At least three points are needed in the region of isotherm where $1/[W(P_0/P)-1]$, P/P_0 plot is linear when so-called multipoint approach of BET theory is applied. In the case of adsorption of N_2, the linear region of $1/[W(P_0/P)-1]$, P/P_0 plot for most solid materials is in the relative pressure region from 0.05 to 0.35. One output of BET theory is to calculate the W_m from the slope and intercept of $1/[W(P_0/P)-1]$, P/P_0 plot:

$$\text{slope} = \frac{c-1}{W_m c} \tag{5}$$

$$\text{intercept} = \frac{1}{W_m c} \tag{6}$$

From Equations (5) and (6) it follows that:

$$W_m = \frac{1}{\text{slope} + \text{intercept}} \tag{7}$$

Knowing the W_m and cross-section area of adsorbate molecule (A_{cs}) the BET specific surface area of adsorbent (S_{BET}) can be calculated:

$$S_{BET} = \frac{W_m N_A A_{cs}}{M \cdot m} \tag{8}$$

where N_A is the Avogadro constant ($6.023 \cdot 10^{23}$ molecules per mole), M is the molar mass of adsorbate and m is the mass of sample.

Often nitrogen cooled to 77 K is used as adsorbate for gas adsorption measurements and BET calculations. N_2 has c values from 50 to 250 depending on the sample and A_{cs} = 1.62 nm [58].

4.1.3.2. *t*-plot method

The *t*-plot method is based on a graph with V_{ads} and the statistical thickness of adsorbed layer, t_{stat}, given on axes. Several equations have been proposed for determining the t_{stat} from measured P/P_0 values during the gas adsorption experiment [59–62]. For the derivation of these equations an assumption has been made that the adsorbed nitrogen in the monolayer has the same density and packing of molecules as for liquid nitrogen. The Harkins-Jura empirical Equation (9), presented here for N_2 adsorption at 77 K, is the most commonly used approximation [61, 62].

$$t_{\text{stat}} = \sqrt{\frac{13.99}{0.034 - \log(P/P_0)}} \tag{9}$$

Experimentally obtained *t*-plots do not form a straight line. Usually, deviations from linearity occur in some regions. Commonly, a straight part in the *t*-plot is found at intermediate and higher relative pressures, corresponding to the unrestricted growth of the adsorption layer in mesopores and external surface. Using the slope in linear region of *t*-plot and N_2 as adsorbate, the external surface area, S_{ext}, of material studied can be calculated according to

$$S_{\text{ext}} = 15.47\text{slope} \tag{10}$$

where the constant = 15.47 is the density conversion factor for nitrogen.

Then the surface area of micropores, S_{micro}, is

$$S_{\text{micro}} = S_{\text{BET}} - S_{\text{ext}} \tag{11}$$

4.1.3.3. Total pore volume

The total pore volume is calculated at relative pressure as close to unity as possible. This allows to presume that all pores are filled with liquid adsorbate. The total pore volume (V_t) can be calculated from the amount of adsroben nitrogen (V_{ads}) using Equation:

$$V_{\text{t}} = \frac{PV_{\text{ads}}V_{\text{molar}}}{\overline{R}\ T} \tag{12}$$

where P is the pressure and V_{molar} is the molar volume of adsorbate (34.7 $\text{cm}^3\ \text{mol}^{-1}$ for N_2 at 77 K)

4.1.3.4. Non-local density functional theory

Classical theories like Dubinin-Radushkevich, Barret-Joyner-Halenda and Horwath-Kawazoe do not describe realistically the filling of micropores and smaller mesopores with adsorbate. Non-local density functional theory (NLDFT) is considered to be more precise in describing the pore size distribution of different materials [63, 64]. NLDFT describes objectively the local structure of liquid condensed compound at curved solid surfaces. The shape of adsorption isotherms of model pores are determined by liquid-liquid and liquid-solid interactions. The relation between the shape of adsorption

isotherm and molecular interactions can be described through equation of generalized adsorption isotherm:

$$N(P/P_0) = \int_{d_{\min}}^{d_{\max}} N(P/P_0, d) f(d) \mathrm{d}d \tag{13}$$

where $N(P/P_0)$ is point in adsorption isotherm, d is the pore width, $N(P/P_0,d)$ is the point corresponding to the pore with width d and $f(d)$ is the function of pore size distribution. The equation of generalized adsorption isotherm assumes that the total isotherm consists of the isotherms of single pores which are multiplied by their distribution $f(d)$ relative to the total pore size distribution.

NLDFT method is usable to characterize micro- and mesoporous carbon, silicon and zeolite materials [63, 64].

4.1.4. Separators in EDLCs

Separators in EDLC separate negatively and positively charged electrodes from each other. Usually, micro-/mesoporous polymer membrane or fibrous material is used for that purpose. Separator must not conduct electrons but must be freely permeable to ions. Separators must be chemically, thermally and mechanically stable and have low density, suitable porosity and pore size distribution to be easily permeable for ions in electrolyte and to minimize the inner resistance of system assembled [65, 66]. The compatibility of the physical and chemical properties of separator and the properties of electrolyte influence strongly the high frequency resistance and therefore, the energy and power densities of EDLC [65]. To achieve the highest energy and power densities, the separator must be as thin and porous as possible, but still have good mechanical stability. Thus, sufficient porosity leads to good ion conductivity and wettability. However, too big pores lead to high leakage currents or short circuits in EDLC [66].

4.1.5. Electrolytes in EDLCs

In general, electrolytes for EDLCs must meet the following requirements [1]:

- *(i)* Wide voltage region of electrochemical stability (i.e. the decomposition voltage of the desired solution). Preferably wider than the intended operational voltage of the capacitor in order to minimize problems arising from adventitious overcharge.
- *(ii)* Minimum viscosity of the electrolyte in order to maximize ionic mobility and resulting conductance.
- *(iii)* Maximum solubility of the electrolyte in solvent to maximize conductance.
- *(iv)* Minimum ion pairing at given practical electrolyte concentrations, again to maximize conductance.

(v) Optimum dielectric permittivity and donor number of the solvent to maximize salt solubility and minimize ion pairing.

All these factors are involved in determining the mobility of the dissociated ions and the concentrations of free charge carriers i.e. the specific conductance of electrolyte at the experimental concentration [1].

Usually, non-aqueous solutions are preferred as electrolytes in EDLCs compared to aqueous solutions (e.g. aqueous solutions of KOH or H_2SO_4). This is so due to the low maximal operational voltage (~1 V) of EDLC based on aqueous electrolyte. Using non-aqueous electrolytes allows to charge EDLC up to 3.5, or even to 4.0 V, increasing energy density from 12 to 16 times, and power density form 3.5 to 4.0 times, respectively [1, 2, 4, 32–34].

The selection of non-aqueous electrolytes is fairly wide, but mostly tetraalkylammonium cation based salts in organic solvents like AN, propylene carbonate (PC), γ-butyrolactone (γ-BL) etc. are used [1, 2, 4, 7–10]. EDLCs based on non-aqueous electrolytes have to be assembled in very pure and dry conditions to avoid dissolving of electrochemically active water and oxygen in electrolyte [1, 2]. The first disadvantage of non-aqueous electrolyte based EDLCs is their higher price compared to EDLCs based on aqueous electrolytes. The difference arises from the costs of salt, solvent and specific apparatus needed to avoid contamination of the EDLC elements with water and oxygen.

4.2. Room-temperature ionic liquids

Room-temperature ionic liquids (RTILs) are salts in liquid phase at temperatures lower than 100 °C [11, 12, 31]. The properties of RTILs differ greatly from the properties of molecular liquids, for example they have no vapor pressure and they have good ion conductivity.

The selection of ionic liquids is relatively wide as there are many different cations and anions to combine with one another resulting ionic liquids with different properties (melting temperature, viscosity, conductivity, hydrophilicity and hydrophobicity etc.). Unfortunately, most ionic liquids have low electrical conductivity (< 5 mS cm^{-1}) and high viscosity (> 50 mPa s). Also, some ionic liquids with good electrical conductivity and low viscosity have narrow region of electrochemical stability [11]. Only some RTILs have high electrical conductivity, wide region of electrochemical stability, good thermal stability, relatively low price and are suitable electrolytes for EDLCs [11, 12]. Detailed information about different physical and electrochemical properties of ionic liquids has been published in Refs. 12 and 31.

4.2.1. Influence of temperature to the electrical conductivity of ionic liquids

At the room-temperature the conductivity of RTILs is relatively low [11, 12, 31], but the rise in temperature increases the conductivity of RTILs [67]. For

that reason, many authors have suggested to use the EDLCs based on RTILs in applications providing elevated working temperature, for example 60 °C [15, 17, 18, 21–26].

In classical solutions of salt in molecular solvents the ions are separated from each other by solvent molecules. The thermodynamical properties of such systems are described mainly through ion-solvent, ion-ion and solvent-solvent interactions. In RTIL there is no solvent and ions are in contact to other ions. Therefore, the thermodynamical properties of RTILs are described through ion interactions, dispersion forces and for some RTILs through formation and strength of hydrogen bonds. Thus, the determination of charge carrier for ionic liquids is somewhat more complex. So far, the so-called "free space model" is the most efficient way to describe the conductivity of RTILs [12]. The model assumes that within the molten salt there are empty spaces constantly fluctuating in size due to thermal motions. To quantify a model, a probability of finding the hole in RTIL is calculated leading to Equations (14) and (15) for diffusion coefficient, D, and specific conductivity, κ:

$$D = \mathrm{A}\exp\left(\frac{-\mathrm{B}}{T - T_0}\right) \tag{14}$$

$$\kappa = \kappa_0 \exp\left(\frac{-\mathrm{B}}{T - T_0}\right). \tag{15}$$

Equations (14) and (15) resemble to the Vogel-Tammann-Fulcher equation (16), describing the temperature dependence of the liquid phase viscosity, η, on temperature, T [69, 70, 71]:

$$\eta = \mathrm{A}\exp\left(\frac{-\mathrm{B}}{T - T_0}\right) \tag{16}$$

where A and B are coefficients characteristic for substance, temperature $T_0 = T_g$ – const., and T_g is the glass transition temperature.

The Vogel-Tammann-Fulcher equation may also be expressed in a number of modified forms. The most frequent modification is based on the temperature dependence of pre-exponential factor, $\kappa_0 = f(T)$, usually as $\kappa_0 = \mathrm{A}T^{-0.5}$ or $\kappa_0 = \mathrm{A}T^{-1}$ [12].

4.2.2. Electrochemical stability of RTILs

Detailed review of properties including electrochemical stability of RTILs has been published in Refs 12 and 31 summarizing the work of many work groups. However, it is somewhat difficult to compare these results because experimental

conditions like purity of RTILs, reference and working electrodes used, potential scan rate etc. are different.

Some generalizations have been made for electrochemical stability of ionic liquids [72]:

(i) The cathodic limiting potential of the RTILs is basically determined by the reduction of the cations.

(ii) Sometimes, if the cathodic stability of the anion is poor, the cathodic limiting potential is determined by the anion reduction and not by the cation reduction.

(iii) The anodic limiting potential of RTILs is basically determined by the oxidation of anions.

(iv) The region of electrochemical stability of aliphatic quaternary ammonium systems based on fluoroanions has the widest region of electrochemical stability compared with that of aromatic systems.

(v) The surface passivation layer originating from the faradaic processes of RTIL on electrode can affect the cathodic and/or anodic limit of system.

4.3. COSMOtherm calculations

To predict the anion charge delocalization in ions studied, the COSMO-RS (conductor-like screening model for real solvents) was chosen [73] and the COSMOtherm software package [74] (version C2.1, revision 01.10) was used. Geometry optimization and generation of COSMO input files were done using the Turbomole software package [75] at the DFT BP TZVP level with full geometry optimization. The COSMO-RS method gives so-called σ-profile, i.e. the distribution of charge density (σ) on a molecular surface [73] applicable to evaluate the charge delocalization in the ionic species [76]. For more detailed analysis [76] a weighted average positive charge density, (WAPS) was introduced and defined as the weighted mean of positive σ values divided by the ion surface area obtained from COSMO-RS output [76]. The surface area segments with negative charge are characterized by positive σ values (due to definition of σ) [73, 76]. The WAPS can be calculated as follows:

$$\mathrm{WAPS} = \frac{\int_{\sigma=0}^{\infty} \sigma \cdot p(\sigma) d(\sigma)}{A \int_{\sigma=0}^{\infty} p(\sigma) d(\sigma)}. \qquad (17)$$

where $p(\sigma)$ is the probability function of σ, and A is the surface area of anion.

4.4. Electrochemical measurement techniques and interpretation of data

4.4.1. Cyclic voltammetry

In the cyclic voltammetry method the potential of system studied is changed linearly with time. The rate at which the potential is changed is called the potential scan rate or scan rate, ν. During the cyclic voltammetry measurements the electrode potential is changed from initial potential E_1 to final potential E_2 and then back to E_1. An oxidation reaction occurring ($Ox + ne^- = Red$) in the system results cyclic voltammogram resembling to one presented in Figure 2.

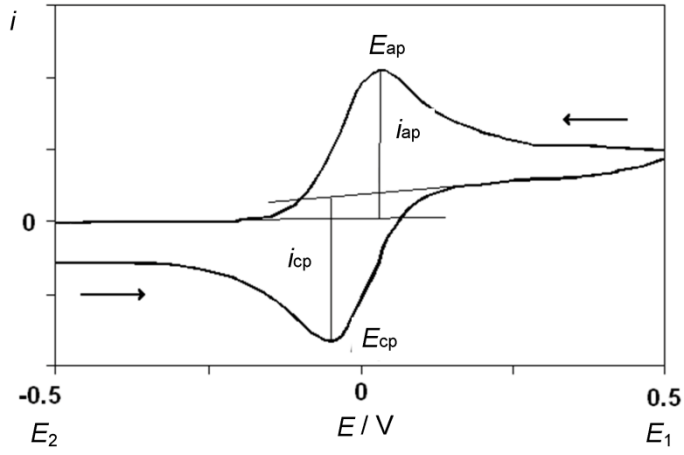

Figure 2. Cyclic voltammogram for a *Red*/*Ox* system.

When the potential is changed in the direction $E_1 \rightarrow E_2$, the oxidant (*Ox*) is reduced and a cathodic (reduction) peak is observed at potential E_{cp}. When a reversed potential scanning is performed the reducer (*Red*) produced in previous process is oxidized and an anodic (oxidation) peak occurs at potential E_{ap}. When the electrochemical process under discussion is totally reversible, the height of peaks at potentials E_{cp} and E_{ap} are equal i.e. $|i_{cp}| = |i_{ap}|$ and the potential of cathodic peak for one electrode process is shifted (58/n) mV towards (n equals the number of electrons transferred in the electrochemical reaction) more positive potential compared to the potential of anodic peak. The formal redox potential $E_{1/2}$ is given as:

$$E_{1/2} = \frac{E_{cp} + E_{ap}}{2} \tag{18}$$

The height of anodic peak is smaller than the height of cathodic peak ($|i_{cp}| > |i_{ap}|$), if the produced reducing agent reacts and gives an electrochemically inactive compound. Partially reversible process results the increase in potential

difference between the cathodic and anodic peak potential. For totally irreversible reduction process the anodic peak corresponding to the oxidation of reducing agent is absent. When no faradaic reactions occur on the electrode surface, no peaks are observed and currents measured can be associated with the electrical double-layer charging only known as ideal capacitive behavior.

In the case of two-electrode system, the total capacitance, C, of EDLC can be calculated according to Equation (19):

$$C = I_{\mathrm{CV}} (dU / dt)^{-1} \tag{19}$$

where U is the cell voltage i.e. the measured potential difference between positively and negatively charged electrode; I_{CV} is the current density, and t is the time. Equation (19) can only be used at low voltage scan rate, where the C is constant, I_{CV} and internal series resistance of test-cell approach to zero. Then the specific gravimetric capacitance for one electrode, C_{CV}, can be calculated from the total capacitance of the test-cell:

$$C_{\mathrm{CV}} = \frac{2C}{m_{\mathrm{am}}} \tag{20}$$

where m_{am} is the active mass of one electrode assuming that the capacitance of both electrodes is the same. In real systems the charge quantities and therefore capacitances of negatively and positively charged electrodes are somewhat different and depend on the size and possible specific adsorption of cations and anions [1, 4, 5, 7–10, 13–15, 17, 27, 28, 53, 65].

4.4.2. Electrochemical impedance spectroscopy

Electrical measurements to evaluate the electrochemical behavior of electrode and/or electrolyte materials of EDLCs are usually conducted with test-cells (EDLCtc) having two identical electrodes. The general approach is to apply an electrical stimulus (a known voltage or current) to the electrodes and observe the response (the resulting current or voltage). It is assumed that the properties of the studied electrode-electrolyte-separator systems are time-invariant and one of the basic purposes of electrochemical impedance spectroscopy is to determine these properties, their interrelations, and dependencies on such controllable variables as electrolyte concentration, temperature, applied static voltage or current bias, etc. [77].

Processes taking place throughout the EDLCtc, when it is electrically stimulated, are mainly associated with the transport of electrons through the electronic conductors, charge transfer on electrode-electrolyte interface and/or transport of ions through electrolyte. The total current depends on the electrical double-layer charging current, faradaic reaction rate on the electrode-electrolyte

interface and on the ohmic resistances of electrode, electrolyte and separator used [65, 77, 78, 79].

The impedance of an electrochemical system is measured by applying a low-amplitude alternative voltage $U(t)$ to a steady state voltage U_0, with

$$U(t) = U_0 \sin(\omega t) \tag{21}$$

where $\omega = 1/(2\pi f)$ – angular frequency; f – frequency, and t – time. This input signal leads to a sinusoidal output current $I(t)$:

$$I(t) = I_0 \sin(\omega t + \theta) \tag{22}$$

where I_0 – initial current, and θ – phase angle between voltage and current, if electrochemical circuit consists from capacitor and resistor connected in series [4, 77]. To simplify calculations, equations (21) and (22) can be rewritten in following forms:

$$I = I_0 e^{j\theta} e^{j\omega t} = I(j\omega) e^{j\omega t} \tag{23}$$

$$U = U_0 e^{j\theta} e^{j\omega t} = U(j\omega) e^{j\omega t} = RI(j\omega) e^{j\omega t} + \frac{1}{C} \frac{I(j\omega) e^{j\omega t}}{j\omega} \tag{24}$$

where $j \equiv \sqrt{-1}$; C is the total capacitance, R is the total resistance and $I(j\omega)$ and $U(j\omega)$ are current and voltage fasors arising from phase angle, respectively. The impedance Z is defined as:

$$Z(\omega) = \frac{U(j\omega)}{I(j\omega)} = R(\omega) + \frac{1}{j\omega C(\omega)} = Z' + jZ'' \tag{25}$$

where Z' and Z'' are the real part and the imaginary part of the impedance, respectively, defined as [4, 77]

$$|Z(\omega)|^2 = (Z')^2 + (Z'')^2 \tag{26}$$

For example the Nyquist plot of a two electrode EDLCtc assembled of 1 M tetrakis(diethylamino)phosphonium tetrafluoroborate, $((C_2H_5)_2N)_4PBF_4$, in AN electrolyte, demonstrating conventional shape for EDLCs using highly porous carbon as electrode material, has been given in Figure 3 [1, 2, 4, 6–10, 13–15, 19–21, 23, 25, 53, 65, 80]. At high frequencies, EDLCtc behave like resistor. At

low frequencies, the imaginary part of the impedance sharply increases and the Nyquist plot tends to a vertical line characteristic of capacitive behavior. In the middle frequency range, the influence of electrode porosity and thickness on the mass-transfer (migration, diffusion) rate of the ions from the electrolyte inside the electrode and separator can be seen [1, 4]. The semicircles observed at high alternative current frequencies have been explained by the resistive-capacitive behavior of carbon electrodes at high frequencies [78, 79]. The distorted shape of these semicircles origins form the distribution of impedance throughout entire electrode without additional ohmic drop [9, 78, 79].

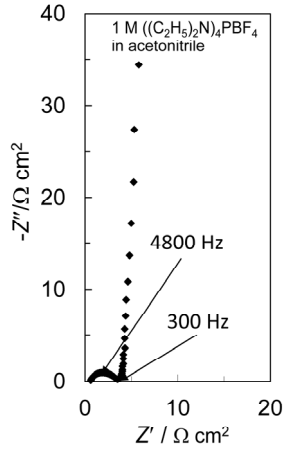

Figure 3. Nyquist plot (-*Z*″,*Z*′ plot) for EDLCtc based on two 2 cm^2 microporous carbon cloth electrodes in 1 M $((C_2H_5)_2N)_4PBF_4$ in AN electrolyte. Frequency range studied is 300 kHz to 1 mHz.

For resistive-capacitive circuit with series resistance, R_s, series capacitance, C_s, parallel resistance, R_p, and parallel capacitance, C_p, components the following relations are valid [80]:

$$R_s = Z'(\omega) \tag{27}$$

$$C_s = -\frac{1}{\omega Z''(\omega)} \tag{28}$$

$$R_p = R_s\left(1+\frac{1}{\tan^2\left(\frac{Z'(\omega)}{Z''(\omega)}\right)}\right) \tag{29}$$

$$C_{\mathrm{p}} = C_{\mathrm{s}}\left(1 + \tan^2\left(\frac{Z'(\omega)}{Z''(\omega)}\right)\right) \tag{30}$$

Maximal specific energy and power for EDLCtc can be estimated from the previous characteristics using Equations (31) and (32), respectively

$$E_{\max} = \frac{U^2 C_{\mathrm{s}}}{2m_{\mathrm{am}}} \tag{31}$$

$$P_{\max} = \frac{U^2}{4R_{\mathrm{s}}m_{\mathrm{am}}} \tag{32}$$

where m_{am} is the active mass of one electrode. It is to be noted, that maximum energy and power of EDLC depend on the square of test-cell voltage, U, and therefore the region of ideal polarizability of electrode in electrolyte studied is of crucial importance. In addition, the capacitance of EDLC should be increased and resistance should be decreased to increase the energy and power densities of EDLCs, respectively.

4.4.3. Calculation of complex power and characteristic relaxation time constant

It is possible to define the real, $C'(\omega)$, and imaginary part, $C''(\omega)$, of series capacitance as:

$$C_{\mathrm{s}}(\omega) = C'(\omega) - \mathrm{j}C''(\omega) \tag{33}$$

where:

$$C'(\omega) = \frac{-Z''(\omega)}{\omega\left|Z(\omega)\right|^2} \tag{34}$$

$$C''(\omega) = \frac{Z'(\omega)}{\omega\left|Z(\omega)\right|^2} \tag{35}$$

The low frequency value of $C'(\omega)$ corresponds to the capacitance of the EDLCtc measured during constant-current charge or discharge, for example. The $C''(\omega)$ corresponds to an energy dissipation by an irreversible electrochemical process that can lead to a hysteresis [4].

The Figure 4a presents the $C'(\omega)$ change vs. frequency, according to Equation (34). The formation of plateau at lower frequencies is common for EDLCtcs based on microporous carbon electrodes and is characteristic of the electrode structure, and the electrode|electrolyte interface [1, 2–4, 6–10, 13–15, 19–21, 23, 25, 53, 65, 80]. The Figure 4b presents the evolution of $C''(\omega)$ vs. frequency, according to Equation (35). The imaginary part of the capacitance goes through a maximum at a characteristic frequency f_0, defining a time constant $\tau_0 = 1/(2\pi f_0)$ for EDLCtc [1, 4]. This time constant has also been described as a dielectric relaxation time [81] characteristic of the whole system. The τ_0 corresponds to the time required to release half of the energy stored in EDLCtc [1, 4] and corresponds to the knee-point frequency at the C_s vs. frequency graphs. However, the determination of the knee-point in C_s vs. frequency graphs is very imprecise, it is not applicable for precise calculations of τ_0 and gives only an estimation of the tendencies in τ_0 changes.

The complex power is defined as

$$S(\omega) = \frac{1}{2}\Delta U(\omega)\cdot\Delta I^{*}(\omega) \tag{36}$$

where the $S(\omega)$ is the apparent or complex power, $\Delta I^{*}(\omega)$ is the conjugated form of the intensity, $\Delta I(j\omega)$; and $\Delta U(j\omega)$ is the complex voltage, the latter two varying according to $j\omega$.

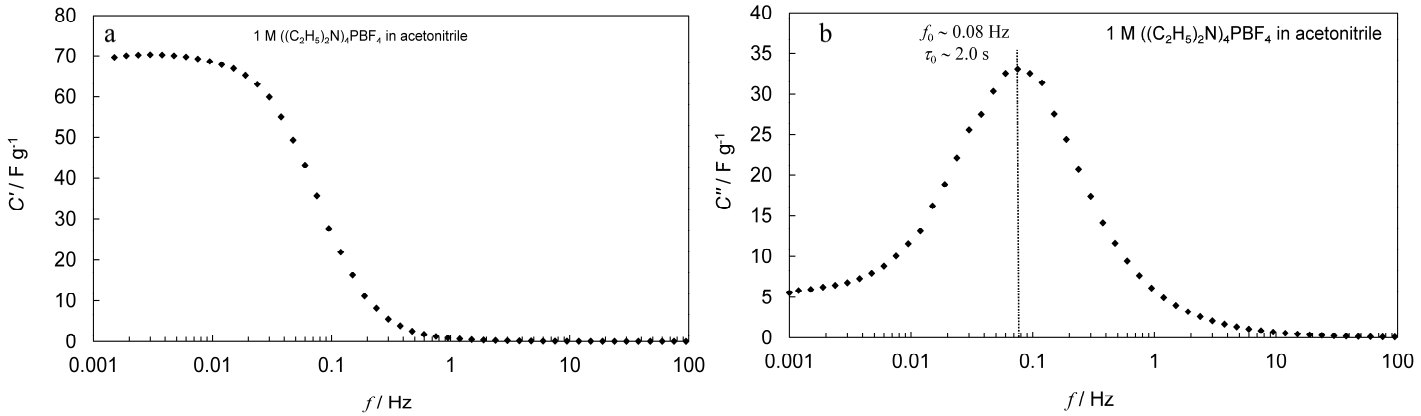

Figure 4. The real part (a) and the imaginary part (b) of capacitance vs. frequency for EDLCtc based on two 2 cm^2 microporous carbon cloth electrodes in 1 M $((C_2H_5)_2N)_4PBF_4$ + acetonitrile electrolyte.

The complex power, $S(\omega)$, can be divided into active, $P(\omega)$, and reactive power, $Q(\omega)$:

$$S(\omega) = P(\omega) + \mathrm{j}Q(\omega) \tag{37}$$

where

$$P(\omega) = \omega C''(\omega)\left|\frac{\Delta U_{\max}}{\sqrt{2}}\right|^2 \tag{38}$$

$$Q(\omega) = -\omega C'(\omega)\left|\frac{\Delta U_{\max}}{\sqrt{2}}\right|^2 \tag{39}$$

and $\Delta U_{\max}$ is the maximal amplitude of alternative current voltage.

Ideal capacitor has no real part as there is only a reactive contribution to the power. Equation (37) has the following form

$$S(\omega) = \mathrm{j}Q(\omega) = -\mathrm{j}\omega C\left(\frac{\Delta U_{\max}}{\sqrt{2}}\right)^2 \tag{40}$$

Ideal resistor has no imaginary part as this component only dissipates energy and the complex power takes the form

$$S(\omega) = \frac{\left(\frac{\Delta U_{\max}}{\sqrt{2}}\right)^2}{|Z'|} \tag{41}$$

with $Z' = R$. Thus, the complex power decreases with the increase in R.

EDLCs demonstrate the resistive behavior at high frequencies and capacitive behavior at low frequencies. Between these two states it behaves like a resistive-capacitive system fitted by (RC) transmission line model [1, 4, 82–84]. In Figure 5 normalized real part, $|P(\omega)|/|S(\omega)|$, and normalized imaginary part, $|Q(\omega)|/|S(\omega)|$, of complex power vs. frequency plots are demonstrated. All the power is dissipated at high frequency ($|P(\omega)|/|S(\omega)| = 1$), when the EDLC has resistive behavior. $|P(\omega)|/|S(\omega)|$ starts to decrease with the decrease in frequency. The normalized imaginary part of the power $|Q(\omega)|/|S(\omega)|$ increases when the frequency is decreased. The same behavior is predicted by the Equation (37), showing that EDLC exhibits only reactive power at $f \to 0$ and thus, $|Q(\omega)|/|S(\omega)| = 1$ [4]. The crossing point of the two plots appears at $|P(\omega)|/|S(\omega)| = |\mathrm{Q}(\omega)|/|S(\omega)|$, when $\theta = -45°$, corresponding to the time constant τ_0.

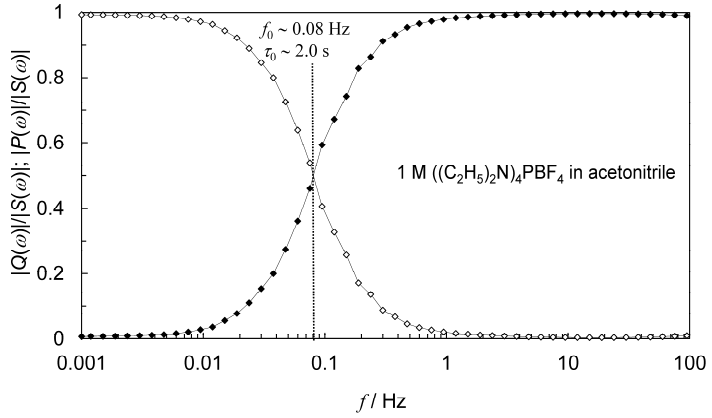

Figure 5. Normalized active power $|P(\omega)|/|S(\omega)|$ and reactive power $|Q(\omega)|/|S(\omega)|$ vs. frequency plots for EDLCtc based on two 2 cm^2 microporous carbon cloth electrodes in 1 M $((C_2H_5)_2N)_4PBF_4$ + acetonitrile electrolyte.

Equations (34), (35), (38) and (39) are used to characterize the influence of various parameters on the time constant, namely, the nature of the electrolyte, the active material parameters in the electrodes and properties of separator [3, 4, 65].

4.4.4. Modelling the electrochemical impedance data with equivalent circuit

To characterize electrical and electrochemical properties of materials and systems under study an equivalent circuit consisting of electrical components can be fitted to the experimental data acquired from impedance spectroscopy measurements. The equivalent circuit completed and selected out is actually the representative of the physical and chemical processes taking place in the experimental system under investigation. Theoretical impedance spectra were calculated by using the equivalent circuit given in Figure 6, where R_{el} is total high-frequency series resistance, C_{ef} is a "true" interfacial capacitance without adsorption effects at high frequencies, and C_{ads} is capacitance corresponding to the slow adsorption processes with adsorption resistance, R_{ads}. The generalized finite Warburg element with a transmission boundary condition, Z_{GFW}, (Equation (42)) has also been introduced into this equivalent circuit and it describes the mass-transport processes of ions in ionic liquid electrolyte, porous electrode and separator matrix [29, 30, 86].

$$Z_{GFW} = R_D \left[\text{ctnh}\left(j\frac{L_{eff}^2}{D_{eff}}\omega \right)^{a_W} \right] \Bigg/ \left(j\frac{L_{eff}^2}{D_{eff}}\omega \right)^{a_W} \tag{42}$$

In Equation (42) R_D is the resistance of diffusion-like processes, L_{eff}^2 / D_{eff} is the so-called mass-transfer frequency parameter where L_{eff} is the effective diffuse layer thickness and D_{eff} is the effective diffusion coefficient of ions, and α_W is the modified Warburg fractional exponent. The impedance $Z_{GFW} = \sigma_{ads}(j\omega)^{-\alpha_W}$, where $\sigma_{ads} = \tau_D^{\alpha_W} C_{ads}^{-1}$ is Warburg constant and τ_D is diffusion relaxation time [87].

The goodness of fit is estimated by the value of the χ^2-function, weighted sum of squares (Δ^2), and by the relative error of each parameter in the equivalent circuit under analysis.

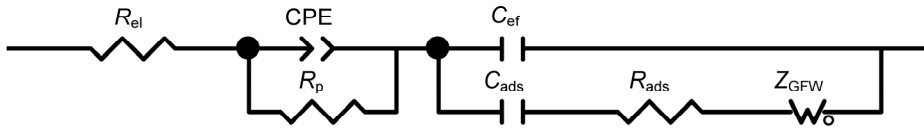

Figure 6. Equivalent circuit consisting of electrical components fitted to the experimental data acquired from impedance spectroscopy. CPE is the constant phase element with the impedance Z_{CPE}; R_p is the parallel resistance; C_{ef} is the "true" interfacial capacitance without adsorption effects calculated at high frequencies; C_{ads} is the so-called adsorption capacitance, corresponding to the slow adsorption processes at $f \to 0$ with adsorption resistance R_{ads}; Z_{GFW} is the Warburg-like diffusion impedance.

5. EXPERIMENTAL

5.1. Electrode materials and preparation of electrodes

In present work *(i)* 775 μm thick electrodes of microporous carbon cloth, MPCC (Ukraine), and *(ii)* 100 μm thick electrodes consisting of TiC (Alfa Aesar, USA) derived carbon (C(TiC), synthesized at 950 °C from TiC according to route described in Section 1.1.2. and in Ref. [13]), 4wt% of polytetrafluoroethylene binder (Sigma-Aldrich, Switzerland) and 3wt% of graphite Timrex KS6 (Timcal, Switzerland) have been used for electrochemical measurements. Both electrode materials have been covered from one side by pure Al layer (~4 μm) by the plasma activated physical vapor deposition method [85]. In Section 6.1. the MPCC and in Section 6.2. the C(TiC) carbon based electrodes have been used to assemble EDLCtcs. The usage of electrodes in Section 6.3. is specified therein.

For surface area and porosity analysis, the N_2 adsorption on both carbon materials was measured at 77 K using the ASAP 2020 (Micromeritics, USA) gas adsorption measurement system. The parameters have been calculated from N_2 sorption isotherms according to Brunauer-Emmett-Teller (BET), *t*-plot and non-local density functional theory (NLDFT). The results demonstrate that both carbon materials have high surface area and are mainly microporous materials with small amount of mesopores (Table I) thus being suitable materials for EDLC electrodes [1–3, 34].

Table I. Results of N_2 sorption measurements at liquid nitrogen temperature of electrode materials used.

	S_{BET}	S_{ext}	S_{micro}	V_t	V_{micro}
MPCC	1560 $m^2\ g^{-1}$	110 $m^2\ g^{-1}$	1450 $m^2\ g^{-1}$	0.92 $cm^3\ g^{-1}$	0.69 $cm^3\ g^{-1}$
C(TiC)	1670 $m^2\ g^{-1}$	60 $m^2\ g^{-1}$	1610 $m^2\ g^{-1}$	0.90 $cm^3\ g^{-1}$	0.75 $cm^3\ g^{-1}$

S_{BET} - surface area calculated by Brunauer-Emmett-Teller theory (P/P_0 = 0.05…0.2); S_{ext}, external or non-micropore surface area by *t*-plot method; S_{micro}, micropore surface area by *t*-plot method; V_t, total pore volume at P/P_0 = 0.999; V_{micro}, micropore volume by *t*-plot method.

5.2. Characteristics of ionic liquids

Six electrochemically interesting ionic liquids consisting of the same 1-ethyl-3-methylimidazolium cation and anions with different electrochemical activity were studied: 1-ethyl-3-methylimidazolium tetrafluoroborate ($EMImBF_4$, Sigma-Aldrich, Switzerland, assay ≥ 99.0%); 1-ethyl-3-methylimidazolium tetracyanoborate ($EMImB(CN)_4$, Merck KGaA, Germany, 99.9%); 1-ethyl-3-methylimidazolium tris(pentafluoroethyl)trisfluorophosphate ($EMImPF_3(C_2F_5)_3$, Merck KGaA, Germany, ≥ 99.0%); 1-ethyl-3-methylimidazolium bis(trifluoro-

methylsulfonyl)imide (EMImN(SO_2CF_3)$_2$, Merck KGaA, Germany, 99.0%); 1-ethyl-3-methylimidazolium bis(fluorosulfonyl)imide (EMImN(SO_2F)$_2$), Solvionic, France, ≥ 99.5%); and 1-ethyl-3-methylimidazolium thiocyanate (EMImSCN, Sigma-Aldrich, Switzerland ≥ 95%).

5.3. Melting point, conductivity and viscosity measurements

The melting points of RTILs were measured with a differential scanning calorimetry on "Diamond DSC" (PerkinElmer, USA) by sealing ~40 mg of the sample in an aluminum pan. The pan and the sample were first cooled to –70 °C and then heated to 100 °C at the temperature ramp rate of 5 °C min^{-1}. The melting point was determined by the maximum of melting peak at differential scanning calorimetry diagram (Table II).

Table II. Physical properties of RTILs used as electrolytes in EDLC.

RTIL	Water content (± 2 ppm)	Melting point (± 0.1 °C)	Conductivity (± 0.04 mS cm^{-2})	Viscosity (± 0.1 mPa s)	WAPS (10^{-5} e A^{-4})
EMImBF_4	19	15.5	15.03	26.7	3.4
EMImB$(CN)_4$	56	12.6	15.91	16.3	1.4
EMIm$PF_3(C_2F_5)_3$	35	2.5	5.35	32.8	0.4
EMImN$(SO_2CF_3)_2$	35	0.8	9.12	32.1	0.8
EMImN$(SO_2F)_2$	N/A	–12.1	17.70	12.5	1.4
EMImSCN	N/A	N/A	22.05	20.0	3.7

The conductivity of ionic liquids was determined by recording the impedance spectra at 0 V of a self-made test-cell with platinum electrodes and filled with 1.5 ml of ionic liquid at room-temperature (22.0 ± 1 °C). The intersection of the impedance spectra and *Z*' axis was treated as the series resistance of the test-cell. The test-cell was calibrated by measuring the resistance for standard 0.001 M and 0.1 M KCl solutions. The conductivities (Table II) for RTILs were calculated using the cell constant (486.5) calculated from calibration measurements.

The viscosity (Table II) of ionic liquids was measured at room-temperature using U-shaped viscosimeter with flow pipe diameter 0.82 mm. The viscosimeter was calibrated with very pure water (MilliQ+ quality).

The water content (Table II) of ionic liquids was measured by Karl-Fischer titration method by using titrant HYDRANAL-Coulomat AG 34836 (Fluka). The water content in EMImSCN and EMImN(SO_2F)$_2$ was undetectable due to very strong interactions between ionic liquid and titrant used. It was verified that the water content did not affect the electrochemical properties of RTILs on

hydrophobic MPCC electrode surface, when $H_2O \leq 200$ ppm [14], thus making all RTILs studied comparable.

5.4. Assembling EDLC test-cells and electrochemical measurements

Two electrodes (2 cm^2) and 25 μm thick cellulose separator TF4425 (Nippon Kodoshi, Japan), were assembled inside a glove box Labmaster sp (MBraun, Germany) at 22.0 ± 1 °C in a clean and dry Ar atmosphere (99.9999%, AGA; O_2 and $H_2O < 0.1$ ppm) into a two-electrode HS test-cell (Hohsen Corp., Japan). Before assembling, the electrodes were held in vacuum for an hour to remove adsorbed water and oxygen form pores of electrode material. The assembled test-cells were filled with RTILs named.

The electrochemical behavior of EDLCs was tested with cyclic voltammetry and electrochemical impedance spectroscopy methods using a 1252A Solartron FRA and SI1287 potentiostat. Impedance spectra were recorded over alternative current frequency range from 3×10^5 to 1×10^{-3} Hz with 5 mV modulation. The tests were carried out at 22.0 ± 1 °C, if not pointed otherwise. The theoretical spectra calculated using equivalent circuit given in Figure 6 have been fitted to the experimental spectra using the non-linear least squares minimization method using ZView for Windows, version 3.2c [77, 87].

6. RESULTS AND DISCUSSION

6.1. The electrochemical behavior of different RTIL based EDLCtcs at room-temperature

6.1.1. Cyclic voltammetry data and analysis for different RTIL based EDLCtcs

The cyclic voltammograms were measured applying the voltage scan rate varied from 1 to 100 mV s^{-1}. The cyclic voltammograms measured with scan rate 1 mV s^{-1} demonstrate that most of systems tested are nearly ideally polarizable up to 2.7 V and voltage scan rates 20 mV s^{-1} (Figure 7a-d). Exceptions are the EMImSCN and $EMImPF_3(C_2F_5)_3$ based EDLCtcs deviating from the ideal capacitive behavior even at 2.0 V (Figure 7a) and potential scan rates higher than 5 mV s^{-1} (Figure 7d), respectively. At cell voltage (U) 3.2 V only $EMImBF_4$ and $EMImB(CN)_4$ ionic liquid based EDLCtcs behave nearly ideally polarizable. The $EMImN(SO_2CF_3)_2$ based EDLCtc is ideally polarizable up to 3.0 V, whereas $EMImN(SO_2F)_2$ based system is only up to 2.7 V.

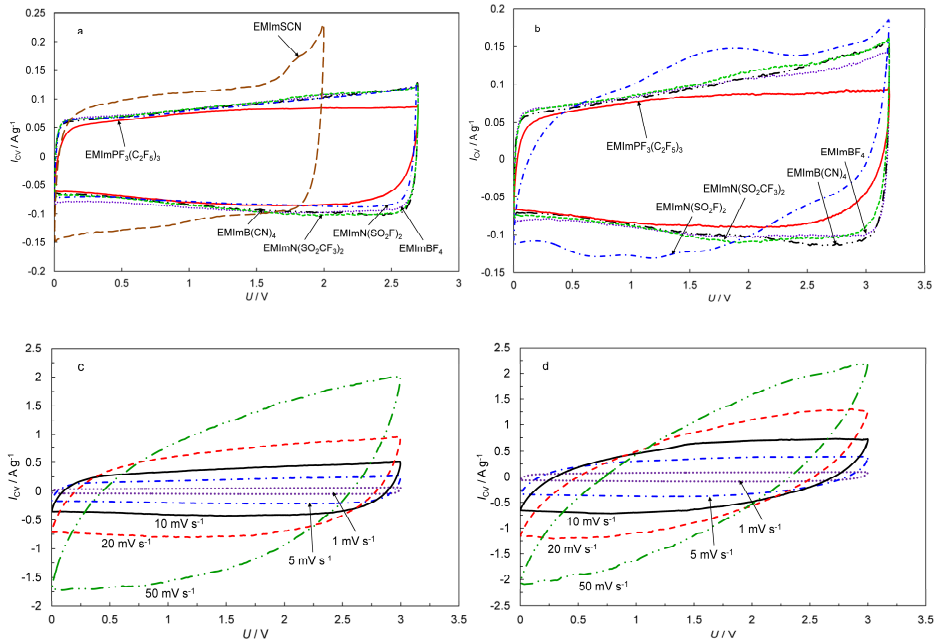

Figure 7. Cyclic voltammograms for different MPCC|RTIL based EDLCtcs (noted in Figures) measured with scan rate 1 mV s^{-1} up to 2.7 V (a); 3.2 V (b); and for MPCC|$EMImBF_4$ (c); and MPCC|$EMImPF_3(C_2F_5)_3$ (d) based EDLCtcs measured with different scan rates up to 3.0 V.

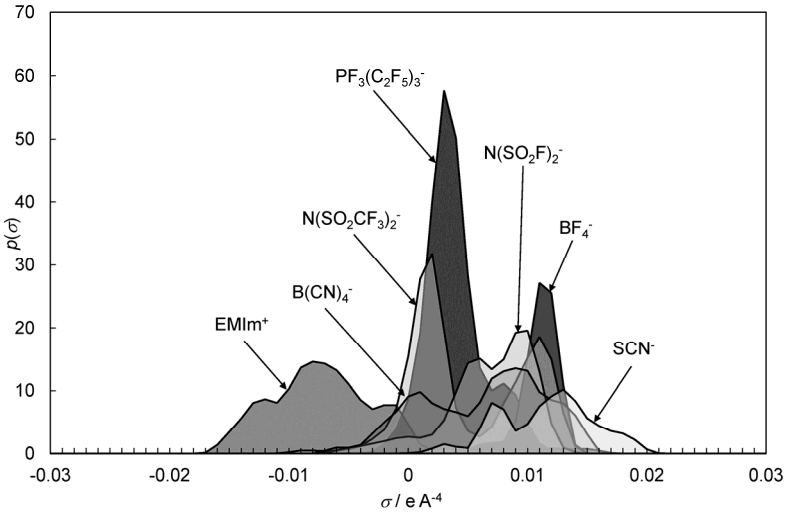

Figure 8. Distribution of charge density (σ) on a molecular surface calculated with COSMO-RS program for RTIL ions dependent on the composition of RTILs studied.

To explain these deviations the σ-profiles, distribution of charge density (σ) on a molecular surface, (Figure 8) and WASP, the weighted average positive charge density, (Table II) for studied ions has been employed. It can be seen that ions used in RTILs studied show only moderate polarization charge densities. The very poor electrochemical stability of SCN^- anion can be explained by the highest WASP value and σ-profile reaching to the most positive values (up to 0.02 e A^{-2}), thus demonstrating the highest polarity (charge localization) [76] from ions studied. Although, the BF_4^- anion also has high WASP value and high narrow peak at relatively high σ values, it has good electrochemical stability (3.2 V). The same can be brought out when $N(SO_2F)_2^-$ and $B(CN)_4^-$ anion based ionic liquids are compared having both WASP = 1.4, but the electrochemical stabilities are different (2.7 V and 3.2 V, respectively). Also, clear differences can be seen in Figure 2, where $N(SO_2F)_2^-$ σ-profile has two separated peaks and reaches more positive values, when peaks for $B(CN)_4^-$ are at lower σ values, broader and low-lying. This demonstrates that unfortunately no simple correlation can be found between polarity of anion in ionic liquid composition and electrochemical behavior of EDLCtc.

Different authors [87–94] have demonstrated that the specific adsorption of ions and partial charge transfer is strongly influenced by various properties of adsorbed ions and sometimes properties of solvent. Thus, it is not generally possible to strictly correlate the electrochemical behavior of ionic liquids composed of same cation and different anions to differences in anion polarity. Some correlation may be noticed for very simple cases only, for example the lower WASP and better electrochemical stability of $N(SO_2CF_5)_2^-$ compared to

$N(SO_2F)_2^-$ arises from the additional charge delocalization caused by additional fluorine atoms in CF_3-group.

Also, it can be seen that for $EMImPF_3(C_2F_5)_3$ based system the distortion effects observed in the voltage switch–over region of cyclic voltammograms cannot be explained by chemical or faradaic reactions at carbon electrode surface but limiting mass–transport steps, because the quite narrow peak near to $\sigma = 0$ axis for $PF_3(C_2F_5)_3^-$ anion in Figure 8 indicates to higher charge delocalization and thus higher stability of anion. This notion is strongly supported by the low conductivity and high viscosity values for $EMImPF_3(C_2F_5)_3$, presented in Table I, and the assumption that different shape of distortion effects on cyclic voltammograms in Figure 7a, b and c compared to other ionic liquid based systems is mainly caused by slow mass-transfer steps.

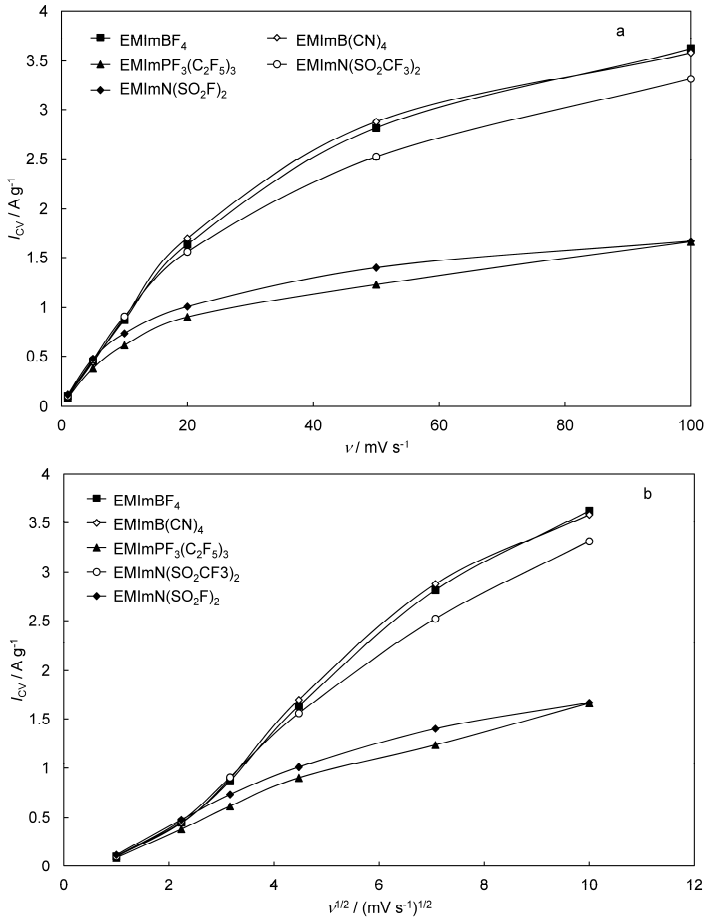

Figure 9. I_{CV}, ν (a) and $I_{CV}, \nu^{1/2}$ (b) at 3.2 V for different MPCC|RTIL based EDLCtcs.

The I_{CV} vs. ν plots at U = 3.2 V (Figure 9a) are nearly linear up to ν = 20 mV s^{-1} and intercepts are nearly 0 for all ionic liquid based EDLCtcs indicating to nearly ideal capacitive behavior of systems studied [9, 27, 28]. In I_{CV}, $\nu^{1/2}$ graph at U = 3.2 V (Figure 9b) the $EMImPF_3(C_2F_5)_3$ and $EMImN(SO_2CF_3)$ based EDLCtcs demonstrate nearly linear $I_{CV}, \nu^{1/2}$ dependence at higher ν indicating to the important role of previously mentioned limiting mass-transfer steps [9, 27, 28, 77]. However, at $U \leq 2.7$ V (not shown for shortness) $EMImN(SO_2CF_3)$ based EDLCtc does not produce linear dependence on $I_{CV}, \nu^{1/2}$ graph. This can be explained by chemical reactions occurring at $U \geq 3.0$ V and blocking of the MPCC electrode surface by reaction products resulting in limitations in mass-transfer and adsorption processes to electrode surface.

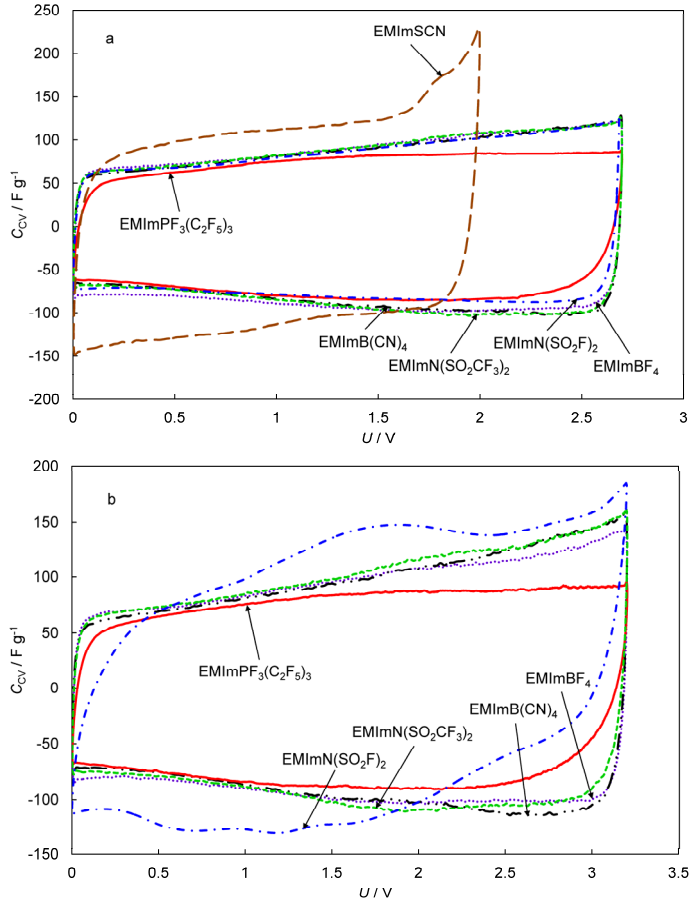

Figure 10. C_{CV},U at 2.7 V (a) and C_{CV},U at 3.2 V (b) for different MPCC|RTIL based EDLCtcs.

The gravimetric capacitance for one electrode (C_{CV}) can be calculated from cyclic voltammograms according to Equations (19) and (20). The C_{CV} of ionic liquid based EDLCtcs (Figure 10c and d) are moderate (~125 F g^{-1}) when compared to highest gravimetric capacitance values achieved on acetonitrile based EDLCtcs (~135 F g^{-1}), published by various authors [4, 9, 53, 65].

6.1.2. Electrochemical impedance spectroscopy data and analysis for different RTIL based EDLCtcs

The Nyquist plots for EDLCtcs studied are presented in Figure 11a and b showing that most MPCC|RTILs interfaces are nearly ideally polarizable, if $U \leq 2.7$ V, demonstrating nearly –90° slope at the low alternative current frequencies. As already seen in cyclic voltammetry graphs MPCC|EMImSCN system is not ideally polarizable even at as low voltages as 2.0 V. From Z'',Z'-plot insets in Figure 11a and b it can be seen that the intersect points of Nyquist plots width Z' axis, corresponding to total high-frequency series resistance, $R_{el} = R_s(f \rightarrow \infty)$, and width of semicircles (corresponding to the high frequency polarization resistance, R_{PHF}) at the high frequencies depend strongly on the anion composition in the ionic liquid.

The semicircles observed have been explained by the resistive-capacitive behavior of carbon electrode|RTIL interface at high frequencies [78, 79]. The distorted shape of these semicircles origins form the distribution of impedance throughout entire electrode with very small additional ohmic drop [9, 78, 79]. The shape of Nyquist plots and high frequency polarization resistance, depend on the conductivity of the electrolyte at the electrode|separator [3, 9, 11, 78, 79] interface and inside the separator [65]. So, it can be explained by low conductivity and high viscosity values of RTILs (Table II) as R_{PHF} is highest for $EMImPF_3(C_2F_5)_3$ ionic liquid based EDLCtc.

The gravimetric series capacitance values, $C_s(f \rightarrow 0)$, (Figure 12a) and gravimetric parallel capacitance values, $C_p(f \rightarrow 0)$, (Figure 12b) calculated from impedance data using Equations (28) and (30) have been plotted against cell voltage applied. For most RTILs the capacitance values do not depend strongly on the composition of anion and the C_s and C_p increase nearly linearly with the increase in U indicating to the increase in Gibbs adsorption with the increase in surface charge density. However, compared to other ionic liquids studied the EMImSCN based EDLCtc shows higher and the $EMImPF_3(C_2F_5)_3$ based EDLCtcs lower C_s values, especially at $U > 1$ V. Also, for most systems studied the obtained ratio $C_p/C_s=1$ is characteristic for ideally polarizable system [10, 13, 53, 65], but for EMImSCN and $EMImPF_3(C_2F_5)_3$ based systems, the C_p/C_s is remarkably smaller than unity. This supports previously proposed assumptions that in EMImSCN based EDLCtcs additional electrochemical reactions are occurring on/inside MPCC electrode matrix and mass-transport limitations are important in $EMImPF_3(C_2F_5)_3$ based EDLCtcs.

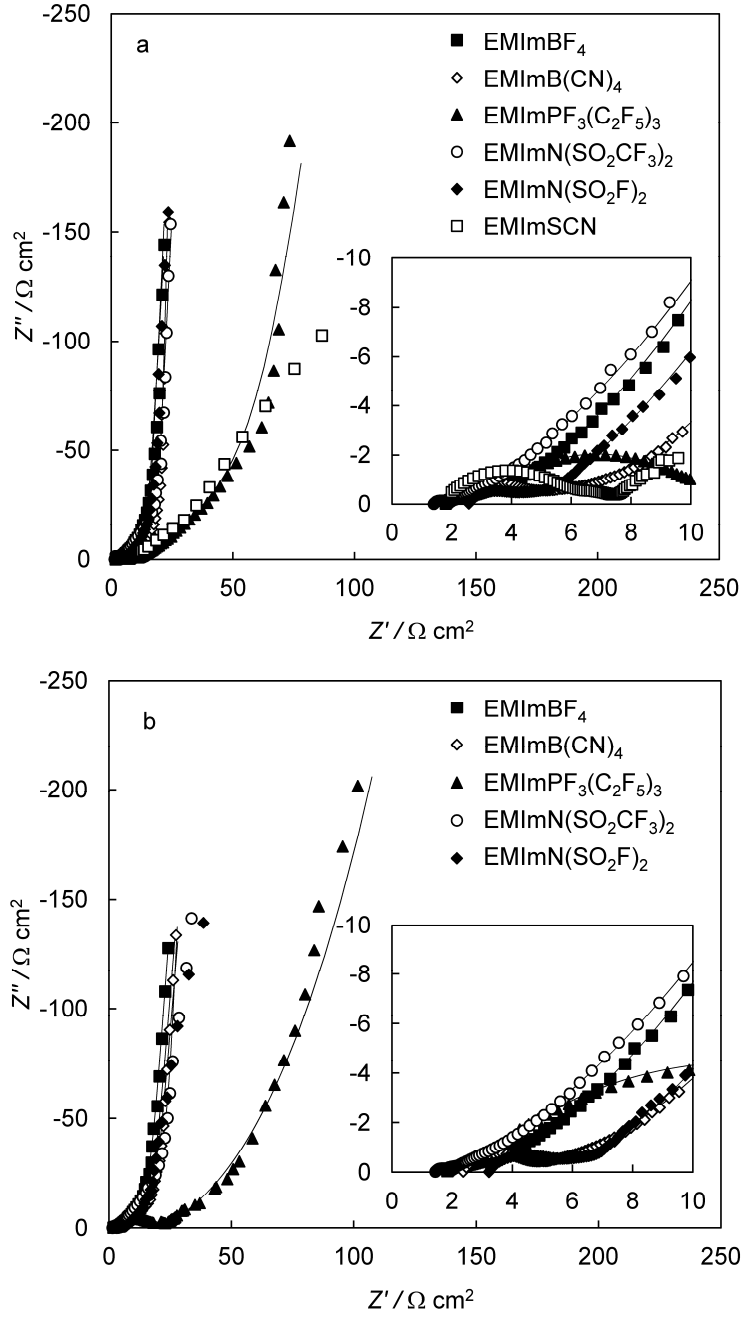

Figure 11. Nyquist plots at 2.0 V (a) and 2.7 V (b) and magnifications of high frequency region as inset for different MPCC|RTIL based EDLCtcs.

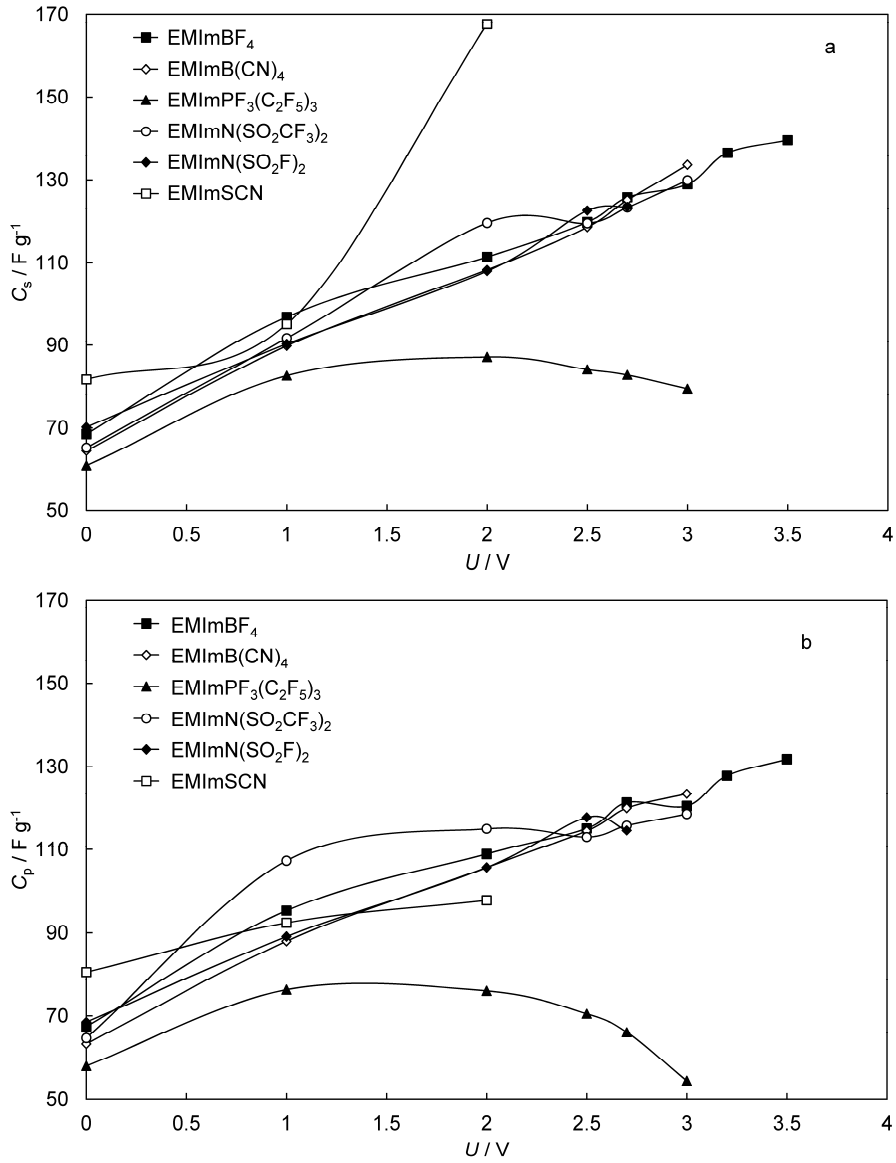

Figure 12. Series capacitance (a) and parallel capacitance (b) dependence on *f* at 2.7 V for different MPCC|RTIL based EDLCtcs.

6.1.3. Modelling the electrochemical impedance spectroscopy data

Visual analysis of the Nyquist (Figure 11a and b) and Bode plots (Figure 13) indicate that at least two characteristic time constants can be distinguished. Therefore the two-sectioned equivalent circuit with seven elements (Figure 6) can be used to calculate the theoretical spectrum within the region of ideal polarizability of MPCC|RTIL based EDLCtcs studied.

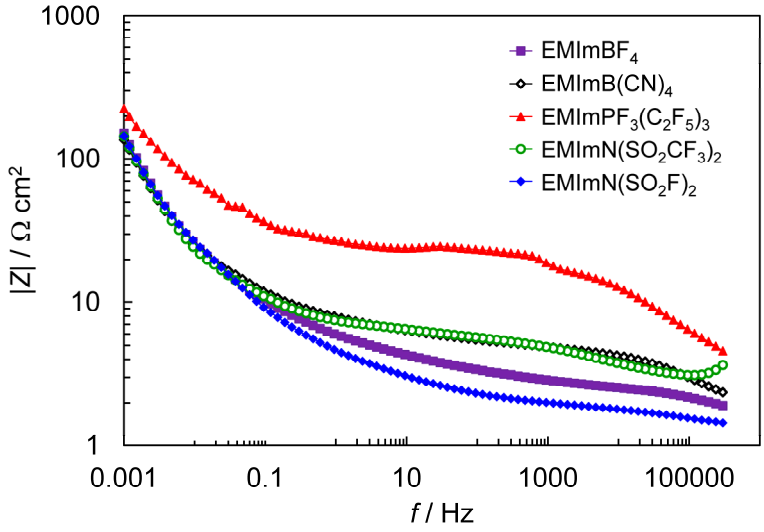

Figure 13. Bode plots for different MPCC|RTIL based EDLCtcs.

It was found that the high frequency section (CPE and R_p) in equivalent circuit describes mainly high frequency behavior of systems studied. In this model, R_{el}, is already introduced and discussed as a total high frequency series resistance (Figure 14) and is nearly independent on voltage applied for all ionic liquids studied.

In Figure 15a and b, it can be seen that C_{ef} is significantly lower compared to C_{ads} indicating to the fact that the low frequency series capacitance, $C_s(f\rightarrow 0)$, is mainly determined by the slow adsorption step of ions on the MPCC electrode surface. The $C_s(f\rightarrow 0)$ (Figure 12a) and C_{ads} values are comparable and both increase somewhat with the increase in cell voltage indicating to the increase in electrostatic adsorption of ions on highly porous electrode surface [29]. The C_{ads} demonstrates some dependence on ionic liquid anion composition being the highest for $EMImB(CN)_4$ and the lowest for $EMImPF_3(C_2F_5)_3$ based system. These results are in good accordance with results obtained on Bi(111) single crystal electrode and can be explained by the differences in the size and surface activity of anions under study [29, 30].

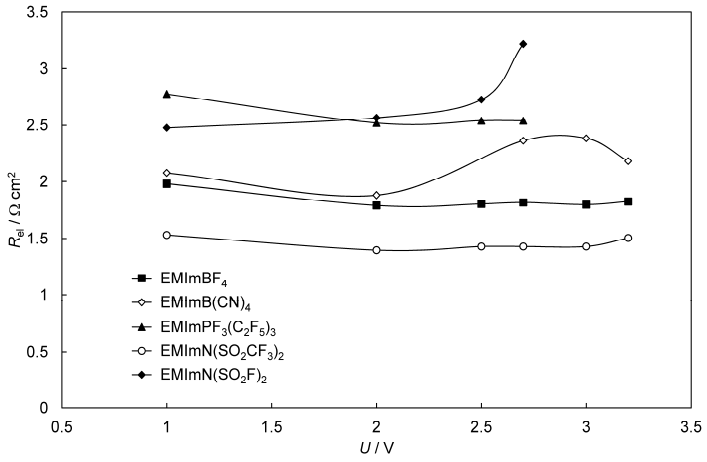

Figure 14. Total high-frequency series resistance for different MPCC|RTIL based EDLCtcs.

The α_W values calculated is nearly 0.5 for all RTILs studied and in region of ideal polarizability does not depend on cell voltage applied. The diffusion resistance, R_D, is significantly higher compared to adsorption resistance, R_{ads}, and increasing somewhat with the rise in voltage (Figure 16a and b, respectively). Discussed effects are especially well pronounced for $EMImPF_3(C_2F_5)_3$ based EDLCtcs probably due to the large anion in the ionic liquid composition, thus indicating to the important role of slow mass-transport processes of ions in porous electrode matrix. The so-called mass-transfer frequency parameter (Figure 16c) for $EMImPF_3(C_2F_5)_3$ is also noticeably higher compared to other ionic liquid based systems, supporting the slow mass-transfer limitation assumptions made already on the basis of cyclic voltammetry data analysis. It must be noted that the dependence of L_{eff}^2 / D_{eff} on anion composition and bulk conductivities of ionic liquids studied are in good agreement.

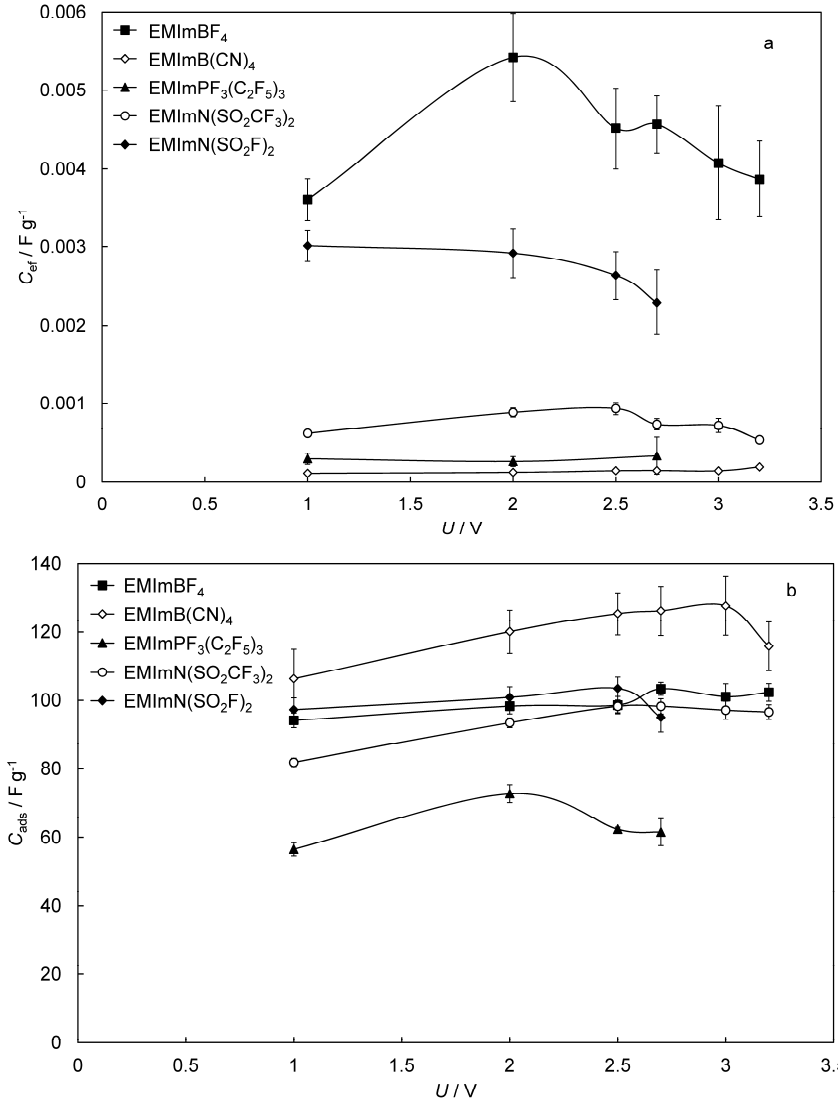

Figure 15. "True" interfacial capacitance (a) and capacitance of adsorption process (b) for different MPCC|RTIL based EDLCtcs.

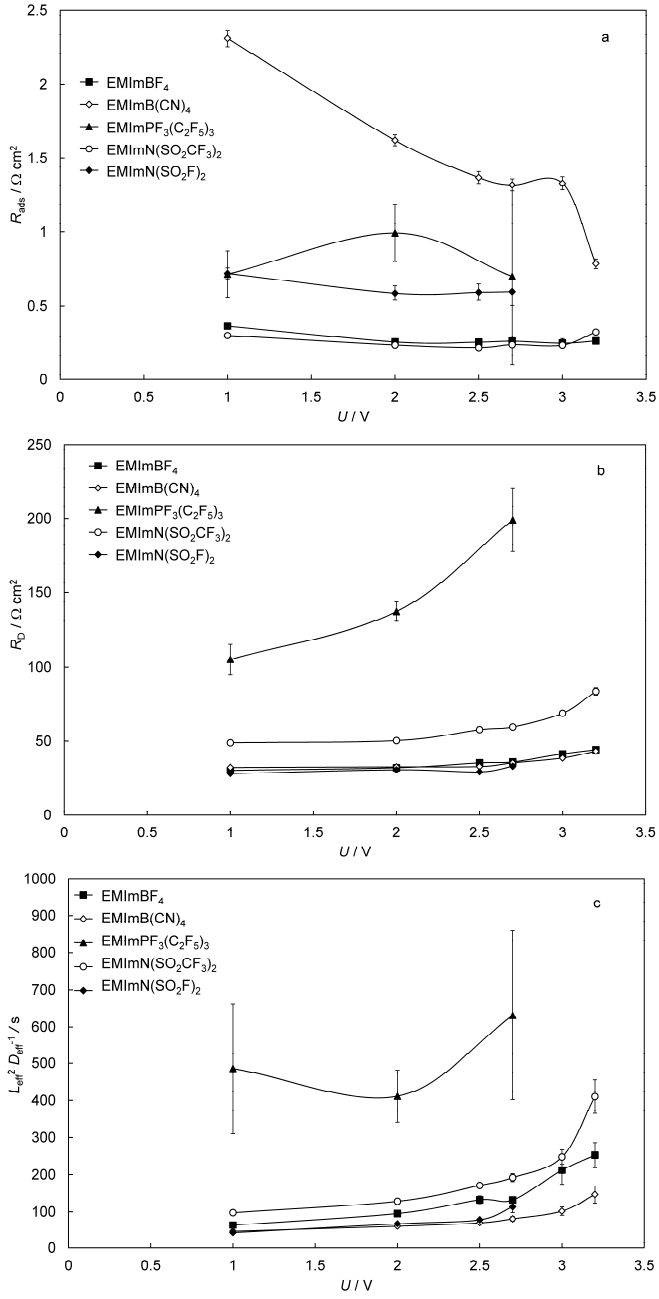

Figure 16. Adsorption resistance (a); resistance of diffusion-like processes (b); and mass-transfer frequency parameter (c) for different MPCC|RTIL based EDLCtcs.

6.2. Influence of temperature on $EMImBF_4$ based EDLCtc electrochemical behavior and physical properties

6.2.1. Influence of temperature on conductivity and viscosity of bulk $EMImBF_4$

Logarithm of specific conductivity, κ, vs. inverse temperature dependencies for $EMImBF_4$ and various electrolytes commonly used in EDLCs are given in Figure 17a. For $EMImBF_4$ there is a nearly linear dependence of log κ on T^{-1} determining the Arrhenius-like activation energy E_{act} = 20.4 kJ mol^{-1}. Noticeably lower values of E_{act} were obtained for 1 M $(C_2H_5)_3CH_3NBF_4$ in AN, PC and equimolecular ethylene carbonate (EC): dimethyl carbonate (DMC): ethyl acetate (EA) solutions. The dynamic viscosity of electrolytes decreases nearly exponentially with increase in temperature (Figure 17b).

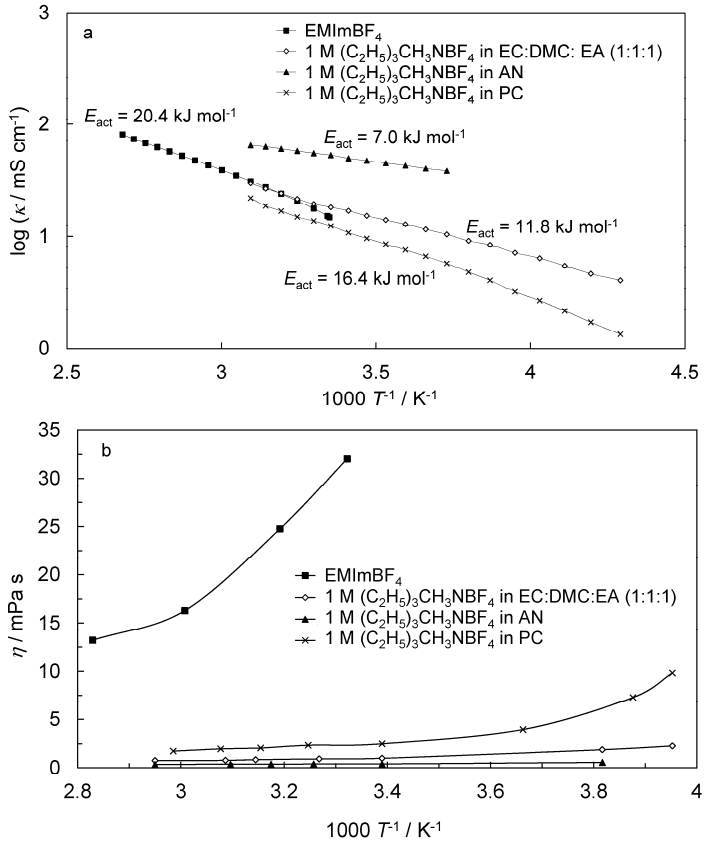

Figure 17. Dependencies of specific conductivity (a) and dynamic viscosity (b) on temperature for electrolytes of EDLCs noted in Figure.

6.2.2. Cyclic voltammetry data and analysis for $EMImBF_4$ based EDLCtcs at different temperatures

The cyclic voltammograms (Figure 18) show that the so-called ideal capacitive behavior for C(TiC)|$EMImBF_4$ based EDLCtcs has been established at $\nu \leq 50$ mV s^{-1} and $U \leq 3.2$ V at temperatures lower than 80 °C. At 25 °C the nearly ideal capacitive behavior can be seen even at $U \leq 3.5$ V (Figure 18 and Figure 19b).

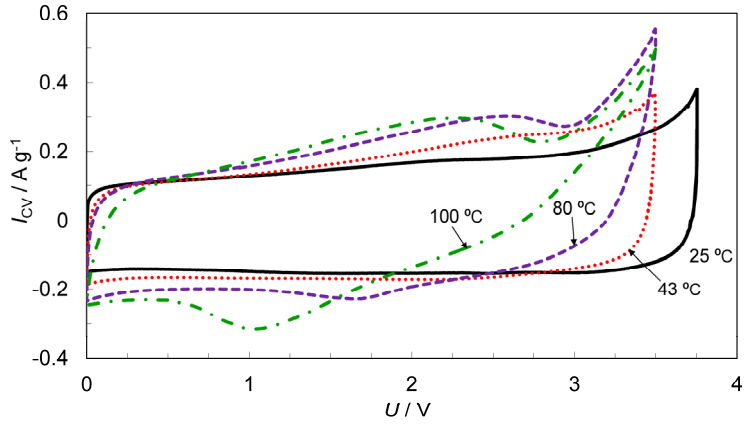

Figure 18. Current density vs. cell voltage plots for C(TiC)|$EMImBF_4$ based EDLCtc at 1 mV s^{-1} and temperatures noted in Figure.

At 80 °C nearly ideal capacitive behavior has been established at voltages lower than 3.0 V. At temperatures higher than 80 °C and $U > 3.0$ V the so-called distortion effects can be seen in the region of voltage switch over (Figure 18), probably caused by decomposition of very small amount of residual water in RTIL, electrochemical reduction of O_2 additives and/or oxidation of functionalities on electrode surface.

At all temperatures tested, the values of C_{CV} for C(TiC)|$EMImBF_4$ based EDLCtc weakly decrease with the rise of voltage scan rate (Figure 19). This effect is more pronounced at higher temperatures indicating to the shifting of adsorption equilibrium towards to the desorption step i.e. the Gibbs adsorption of ions decreases with increase in temperature. Thus, the nearly equilibrium values of capacitance can be obtained at temperatures ≤ 43 °C and only at moderate voltage scan rates ($\nu \leq 5$ mVs^{-1}) indicating that the establishment of the adsorption equilibrium is quite slow process for C(TiC)|$EMImBF_4$ interface, especially at higher temperatures. In the region of $U \geq 3.2$ V and $\nu \leq 10$ mV s^{-1} the values of capacitance increase with the rise in temperature from 25 °C to 80 °C. The deviation of the EDLCtc from the so called ideally polarizable electrode model and the maxima in I_{CV},U- and C_{CV},U-plots (Figure 19b) at low voltage scan rates $\nu \leq 1$ mV s^{-1} and temperatures higher than 43 ºC can be

explained by the electrochemical decomposition of residual H_2O and electroreduction of O_2 traces in RTILs. At 100 °C there are anomalous effects for systems under study even at voltage 1.9 V, associated to the faradaic processes taking place at C(TiC)|EMImBF$_4$ interface.

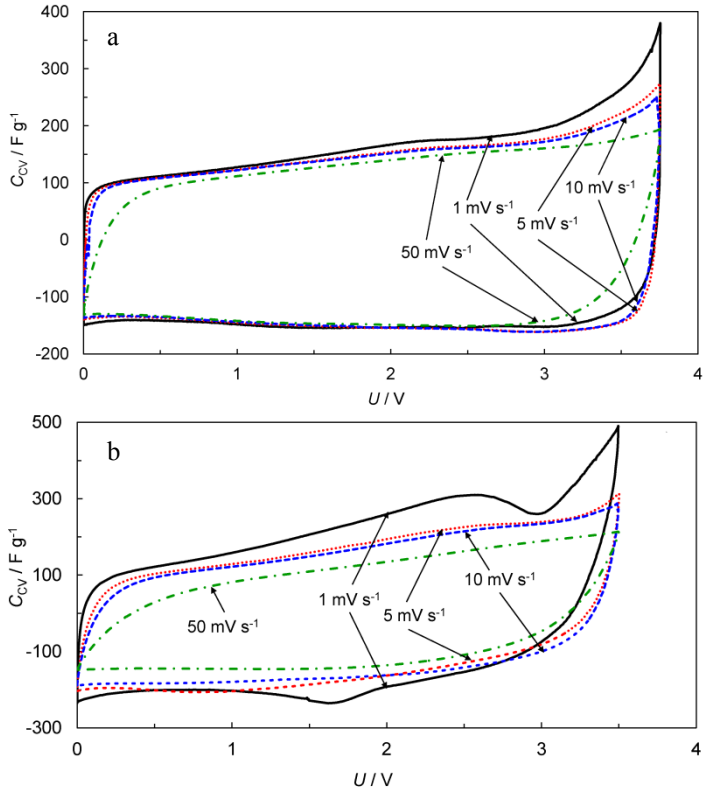

Figure 19. Gravimetric capacitance vs. cell voltage plots for C(TiC)|EMImBF$_4$ based EDLCtcs at temperatures 25°C (a) and 80°C (b) calculated for scan rates noted in Figures.

6.2.3. Electrochemical impedance spectroscopy data and analysis for EMImBF$_4$ based EDLCtcs at different temperatures

According to the data in Figure 20a and b the EMImBF$_4$ based EDLCtcs have fairly conventional behavior at temperatures ≤ 43°C. At 25 °C, the nearly ideal capacitive behavior has been established even at $U \geq 3.2$ V. The high-frequency R_{el} values calculated at $Z''(\omega) \rightarrow 0$ are somewhat lower than those obtained for other similar systems, discussed in papers [15, 19, 20, 23, 25]. For C(TiC)|EMImBF$_4$ based EDLCtcs the previously discussed (Section 3.2.2.) depressed semicircles can also be observed. At higher temperatures (e.g. 80 °C) and voltages the width of high-frequency semicircle (i.e. R_{PHF}) increases with

temperature, indicating to the increasing role of surface "blocking" by the reaction intermediates (e.g. adsorbed gas components inside the C(TiC) electrode and TF4425 separator), leading to the decrease of effective conductivity of electrolyte inside the porous systems (Figure 20c). It has to be noted that, if these anomalies would be caused by the occurrence of the diffusion-like processes inside the electrode, then R_{PHF} should be independent of voltage applied. The increase in R_{PHF} with voltage clearly indicates to faradaic processes at $T \geq 80$ °C and $U \geq 3.0$ V.

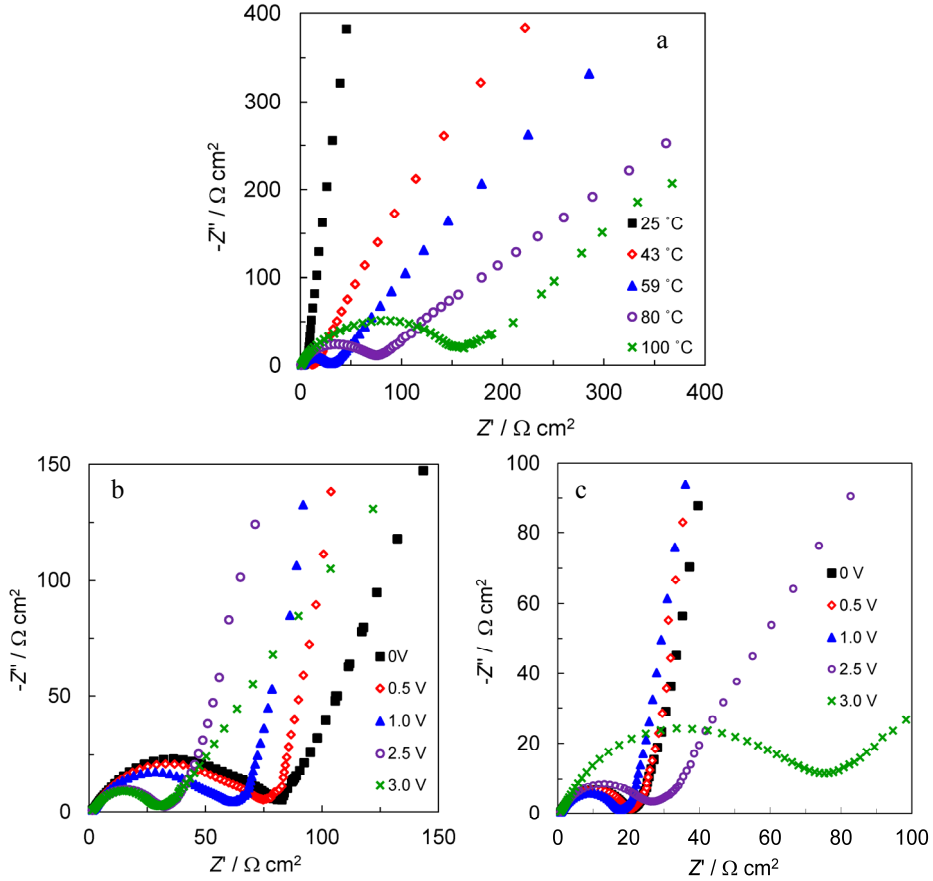

Figure 20. Nyquist plots for C(TiC)|EMImBF$_4$ based EDLCtcs at 3.0 V and temperatures noted in Figure (a); at 59 °C (b); and at 80 °C and voltages noted in Figure (c).

The R_{el} is nearly independent of voltage even at higher temperatures, explained by the absence of quick faradaic processes at the C(TiC)|EMImBF$_4$, interface. At fixed voltage, R_{el} decreases weakly with increase in temperature, agreeing with molar conductivity vs. inverse temperature dependence and moderate activation energy values for EMImBF$_4$, given in Figure 17a.

The C_s calculated according to Equation (28) from impedance data for C(TiC)|EMImBF$_4$ based EDLCtcs at fixed temperature and voltage applied are given in Figure 21a and b, respectively. At temperatures lower than 43 °C, C_s increases with voltage, if $U \leq 3.0$ V, but at voltages higher than 3.2 V, the decrease of C_s takes place due to the blocking effect of pores in electrode with adsorbed gases (generated during faradaic processes). At 3.0 V the C_s values are independent of temperature, if $T \leq 59$ °C (Figure 21b). However, the plateau is formed at lower frequencies in C_s, f-plot indicating to the lengthening of τ_0 corresponding to the knee-point frequency in Figure 21a and b. At higher temperatures C_s decreases because of the shifting of adsorption equilibrium toward desorption process and blocking of microporous carbon electrode matrix by gaseous components that form during the faradic redox processes and adsorb/absorb at electrodes. At temperatures higher than 80 °C, the limiting capacitive behavior exists only at lower electrode voltages ($U \leq 1.9$ V) (Figure 20b and Figure 21b). Therefore, the C(TiC)|EMImBF$_4$ based EDLCtc deviates from ideal capacitive behavior with the increase in voltage and temperature.

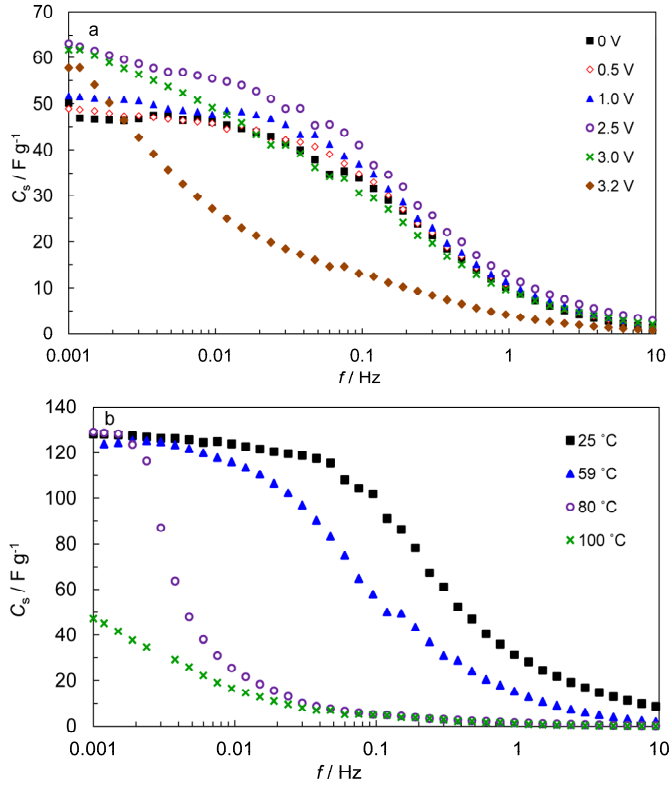

Figure 21. Series capacitance vs. frequency plots for C(TiC)|EMImBF$_4$ based EDLCtc at 43°C and different voltages (a); and at 3.0 V and temperatures noted in Figure (b).

These conclusions are in a good agreement with C_p vs. frequency dependences (Figure 22a and b) calculated from the electrochemical impedance spectroscopy data according to Equation (30), demonstrating that $C_p(\omega \rightarrow 0)$ values decrease with the rise in temperature and at fixed temperature (59 °C) C_p values are maximal at 2.5 V. At 25 °C C_p regularly increases with the increase in voltage.

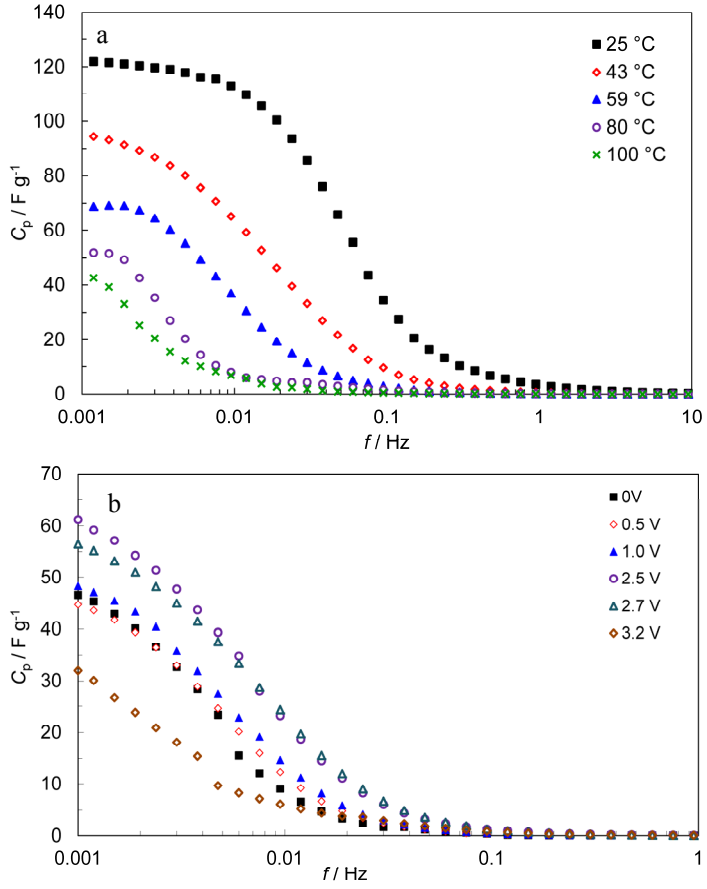

Figure 22. Parallel capacitance vs. frequency dependencies for C(TiC)|EMImBF$_4$ based EDLCtc at 3.0 V and temperatures noted in Figure (a); and at 59°C and voltages noted in Figure (b).

The dependence of ratio C_p/C_s on frequency is shown in Figure 23. For the ideally polarizable system $C_p/C_s = 1$, thus, the C(TiC)|EMImBF$_4$ interface can be taken as a nearly ideally polarizable interface only at $T \leq 43$ °C and $U < 3.0$ V [1, 7, 9, 10, 12, 79]. The ratio values $C_p/C_s < 1$ at temperatures higher than 59 ºC and $U \geq 3.0$ V indicate the noticeable deviation of C(TiC)|EMImBF$_4$ based EDLCtc from the ideally polarizable interface at test conditions.

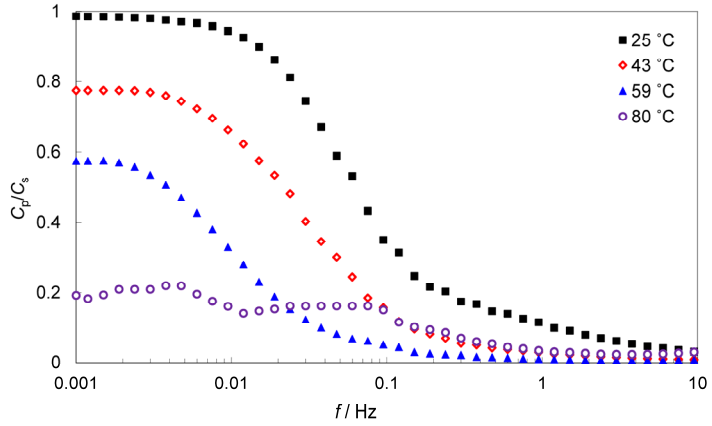

Figure 23. Ratio C_p/C_s vs. frequency dependencies for C(TiC)|EMImBF$_4$ based EDLCtcs at U = 3.0 V and temperatures noted in Figure.

6.3. Comparison of RTILs and other electrolytes in EDLCtcs

For comparison, six different EDLCtcs have been chosen (1) MPCC|EMImBF$_4$ at 22 ± 1 °C [14]; (2) MPCC EMImB(CN)$_4$ at 22 ± 1 °C [14]; (3) C(TiC)|1 M ((C$_2$H$_5$)$_2$N)$_4$PPF$_6$ in AN at 22 ± 1 °C [8]; (4) C(TiC)|1 M triethylmethylammonium tetrafluoroborate, Et$_3$MeNBF$_4$, in AN at 22 ± 1 °C; (5) C(TiC)|0.4 M N,N-dimethyl–1,4-diazabicyclo[2,2,2]octanediium tetrafluoro-borate, CH$_3$N(C$_2$H$_4$)$_3$NCH$_3$(BF$_4$)$_2$, in γ-butyrolactone (γ-BL) at 22 ± 1 °C [95]; (6) C(TiC)|EMImBF$_4$ at 25 ± 1°C [13].

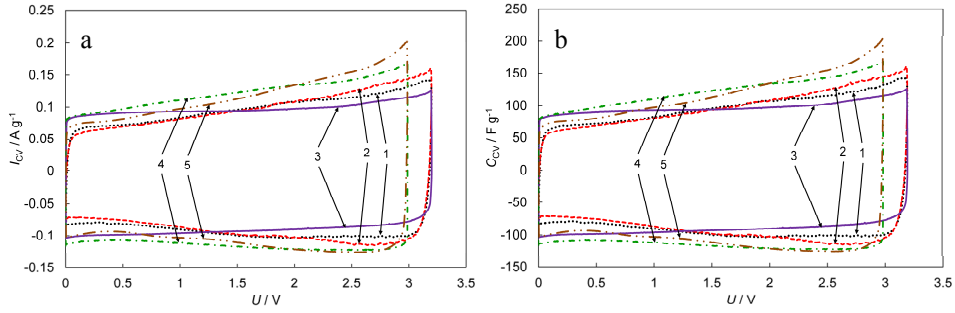

Figure 24. Current density vs. voltage (a) and capacitance vs. voltage (b) for EDLCtcs based on (1) MPCC|EMImBF$_4$ at 22 ± 1 °C; (2) MPCC|EMImB(CN)$_4$ at 22 ± 1 °C; (3) C(TiC)|1 M ((C$_2$H$_5$)$_2$N)$_4$PPF$_6$ in AN; (4) C(TiC)|1 M Et$_3$MeNBF$_4$, in AN at 22 ± 1 °C; (5) C(TiC)|0.4 M CH$_3$N(C$_2$H$_4$)$_3$NCH$_3$(BF$_4$)$_2$ in γ-BL at 22 ± 1 °C.

All cyclic voltammograms for EDLCtcs noted in Figure 24a have fairly conventional shapes. The slopes of the mid-region part of cyclic voltammograms are different for EDLCtcs studied indicating to the quickest Gibbs adsorption (quickest increase of capacitance) for C(TiC)|0.4 M $CH_3N(C_2H_4)_3NCH_3(BF_4)_2$ in γ-BL and slowest for C(TiC)|1 M $((C_2H_5)_2N)_4PPF_6$ in AN. This demonstrates that the influence of voltage on Gibbs adsorption of ions is different, depending strongly on the chemical composition, structure and charge of ions adsorbed on the electrode surface. Differential capacitance, C_{CV}, values (Figure 24b) calculated according to Equations (19) and (20) are highest for the C(TiC)|1 M Et_3MeNBF_4 in AN based EDLCtc.

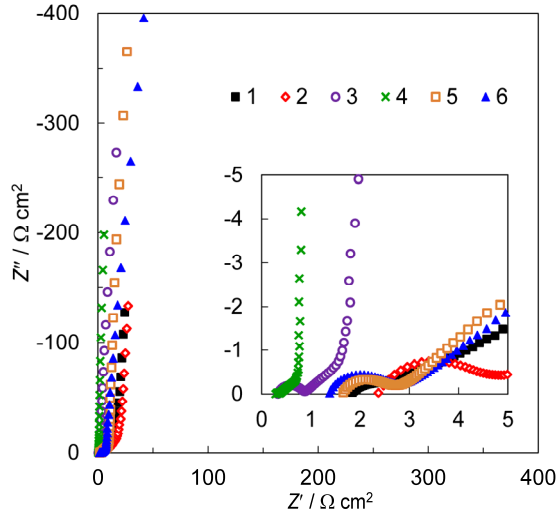

Figure 25. Nyquist plots at 2.7 V for EDLCtcs based on (1) MPCC|$EMImBF_4$ at 22 ± 1 °C; (2) MPCC|$EMImB(CN)_4$ at 22 ± 1 °C; (3) C(TiC)|1 M $((C_2H_5)_2N)_4PPF_6$, in AN at 22 ± 1 °C; (4) C(TiC)|1 M Et_3MeNBF_4, in AN at 22 ± 1 °C; (5) C(TiC)|0.4 M $CH_3N(C_2H_4)_3NCH_3(BF_4)_2$, in γ-BL at 22 ± 1 °C; (6) C(TiC)|$EMImBF_4$ at 25 °C.

Also, the shape of Nyquist plots is conventional for all EDLCtcs in Figure 25 demonstrating nearly –90° slope at low frequencies and already discussed depressed semicircle at high frequencies. The R_{el} and the R_{PHF} depend strongly on the electrolyte and electrode used in EDLCtc being the lowest for C(TiC) based electrode immersed in Et_3MEBF_4 and $(C_2H_5)_2N)_4PPF_6$ electrolytes dissolved in AN. The differences in the resistive behavior of EDLCtcs may arise from the variation in thickness, chemical composition of surface functionalities, pore structure and distribution of electrode materials, compatibility of these properties with electrolyte used. Conductivity and viscosity of electrolyte in electrode matrix, dependent on the chemical composition of electrolyte and structure of electrode have also moderate influence on the EDLCtc behavior [1–4, 7–10, 13, 14, 32–34, 53].

To compare these EDLCtcs from practical aspect, the C_s values for EDLCtcs, given in Figure 26, are presented at the maximal operational voltage, U_{max}, of every EDLCtc, i.e. at the maximum voltage at which the EDLCtc can be operated without remarkable irreversible damage. EDLCtcs based on MPCC|EMImBF$_4$, MPCC|EMImB(CN)$_4$, C(TiC)|0.4 M $CH_3N(C_2H_4)_3NCH_3$-$(BF_4)_2$, in γ-BL and C(TiC)|EMImBF$_4$ demonstrate series capacitance (from 130 to 140 F g^{-1}) exceeding the capacitance of EDLCtcs based on C(TiC)|1 M Et_3MeNBF_4 in AN (115 F g^{-1}) and C(TiC)|1 M $((C_2H_5)_2N)_4PPF_6$ in AN (80 F g^{-1}). However, the plateau in the low frequency region is formed at the highest frequencies for the C(TiC)|1 M Et_3MeNBF_4 in AN based EDLCtc suggesting that the τ_0 values corresponding to the frequency at the knee-point in $C_s f$-plot are shortest for this EDLCtc. To confirm that, $|P(\omega)|/|S(\omega)|;|Q(\omega)|/|S(\omega)|$ vs. frequency plots are presented in Figure 27 and τ_0 values are calculated according to description in Section 1.5.3. The shortest relaxation times have been established for (i.e. the stored charge can be released fastest from) C(TiC) electrode and 1 M Et_3MeNBF_4 in AN and 1 M $((C_2H_5)_2N)_4PPF_6$ in AN electrolyte based EDLCtcs. As it can be noticed, the τ_0 is also strongly dependent on the properties of electrode, electrolyte and their compatibility.

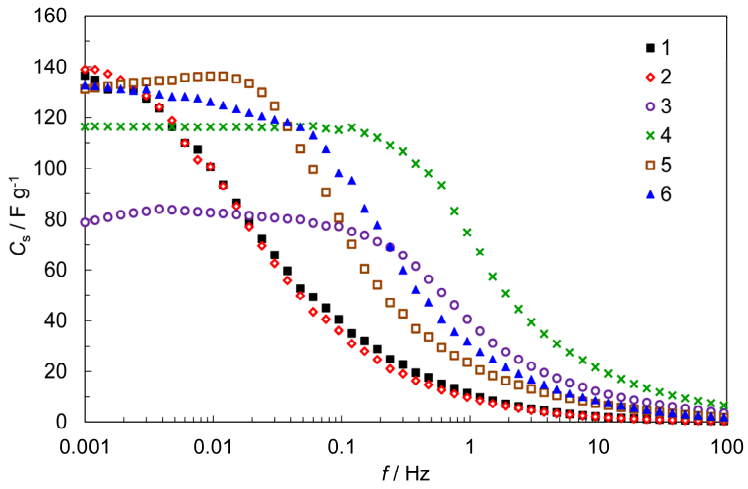

Figure 26. Gravimetric series capacitance vs. frequency at maximal operational voltage for EDLCtcs based on (1) MPCC|EMImBF$_4$ at 22 ± 1 °C (U_{max} =3.2 V); (2) MPCC|EMImB(CN)$_4$ at 22 ± 1 °C (U_{max} =3.2 V); (3) C(TiC)|1 M $((C_2H_5)_2N)_4PPF_6$, in AN at 22 ± 1 °C (U_{max} =3.2 V); (4) C(TiC)|1 M Et_3MeNBF_4, in AN at 22 ± 1 °C (U_{max} = 2.7 V); (5) C(TiC)|0.4 M $CH_3N(C_2H_4)_3NCH_3(BF_4)_2$, in γ-BL at 22 ± 1 °C ($U_{max}$ =3.0 V); (6) C(TiC)|EMImBF$_4$ at 25 °C (U_{max} = 3.2 V).

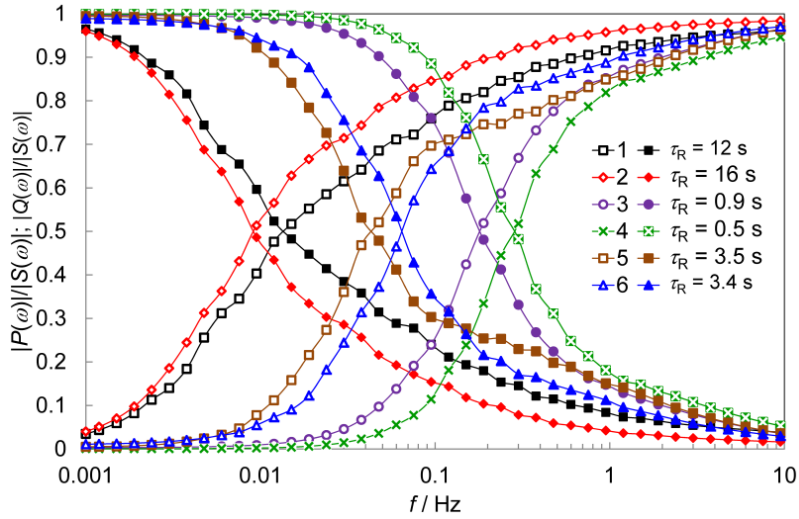

Figure 27. $|P(\omega)|/|S(\omega)|;|Q(\omega)|/|S(\omega)|$ vs. frequency plots at 2.7 V for EDLCtcs based on (1) MPCC|$EMImBF_4$ at 22 ± 1 °C; (2) MPCC|$EMImB(CN)_4$ at 22 ± 1 °C; (3) C(TiC)|1 M $((C_2H_5)_2N)_4PPF_6$, in AN at 22 ± 1 °C; (4) C(TiC)|1 M Et_3MeNBF_4, in AN at 22 ± 1 °C; (5) C(TiC)|0.4 M $CH_3N(C_2H_4)_3NCH_3(BF_4)_2$, in γ-BL at 22 ± 1 °C; (6) C(TiC)|$EMImBF_4$ at 25 °C.

The maximum specific energy and power at U_{max} are presented in Figure 28. As it can be expected from Equation (31), the best energy performance can be expected from the EDLCtcs with highest capacitance values. In accordance to Equation (32), the best power performance is established for EDLCtcs with lower R_{el} values. Again, dependencies of EDLCtcs electrochemical behavior on electrode material and electrolyte characteristics are clearly visible. The use of RTILs instead of organic solvent based electrolytes has increased the energy density of EDLCtcs nearly 2 times but decreased the power density at least just as much. As emphasized by many authors, the high power density and short τ_0 of EDLCs are favorable instead of higher energy values. This is due to the fact that there is wide selection of batteries with specific energy up to 100 times higher compared to EDLCtcs studied [1, 2, 32–34, 96] making the C(TiC)|$EMImBF_4$ based EDLCtc the most desirable of RTIL based EDLCtcs.

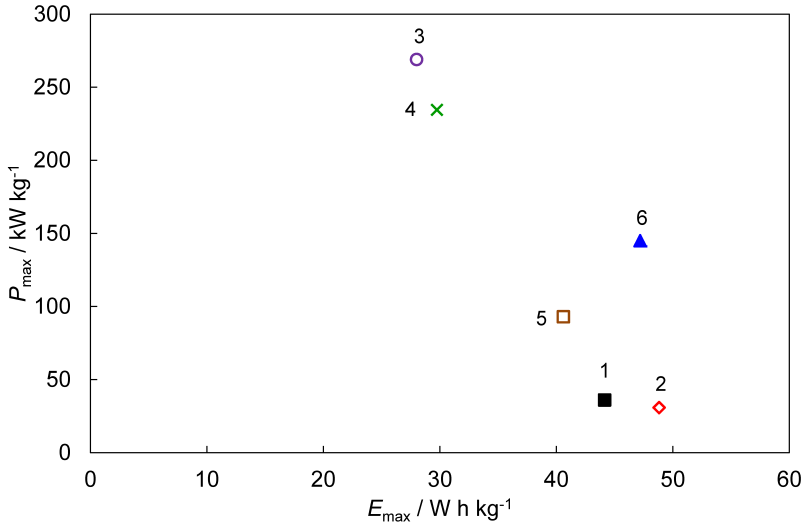

Figure 28. Maximal specific power vs. maximal specific energy for EDLCtcs based on (1) MPCC|EMImBF$_4$ at 22 ± 1 °C U_{max} =3.2 V; (2) MPCC|EMImB(CN)$_4$ at 22 ± 1 °C and U_{max} =3.2 V; (3) C(TiC)|1 M ((C$_2$H$_5$)$_2$N)$_4$PPF$_6$, in AN at 22 ± 1 °C and U_{max} = 3.2 V; (4) C(TiC)|1 M Et$_3$MeNBF$_4$, in AN at 22 ± 1 °C and U_{max} = 2.7 V; (5) C(TiC)|0.4 M CH$_3$N(C$_2$H$_4$)$_3$NCH$_3$(BF$_4$)$_2$, in γ-BL at 22 ± 1 °C and U_{max} =3.0 V; (6) C(TiC)|EMImBF$_4$ at 25 °C and U_{max} = 3.2 V.

7. SUMMARY

Different room-temperature ionic liquids (RTILs) (1-ethyl-3-methylimida-zolium tetrafluoroborate ($EMImBF_4$), 1-ethyl-3-methylimidazolium tetracyano-borate ($EMImB(CN)_4$), 1-ethyl-3-methylimidazolium tris(pentafluoroethyl)-trisfluoro-phosphate ($EMImPF_3(C_2F_5)_3$), 1-ethyl-3-methylimidazolium bis(tris-fluoro-methylsulfonyl)imide ($EMImN(SO_2CF_3)_2$), 1-ethyl-3-methylimidazolium bis(fluorosulfonyl)imide ($EMImN(SO_2F)_2$) and 1-ethyl-3-methylimidazolium thiocyanate (EMImSCN)) were studied as an electrical double-layer capacitor test-cell (EDLCtc) electrolytes. Microporous carbon cloth electrodes and cellulose separator TF4425 were used to complete the EDLCtc. The $EMImBF_4$ and $EMImB(CN)_4$ based EDLCtcs demonstrated widest region of electrochemical stability (3.2 V), resulting highest capacitance (~125 F g^{-1}), energy (45 and 49 W h kg^{-1}, respectively) and power densities (36 and 31 kW kg^{-1}, respectively). Thus, the electrochemical characteristics of EDLCtcs depend strongly on the chemical composition, structure and polarizability of the anion in RTIL and are associated to physical properties like conductivity and viscosity of electrolyte used.

To study the influence of temperature on the electrochemical properties of RTILs the $EMImBF_4$ based EDLCtcs were assembled using TiC derived carbon electrodes (C(TiC)) and TF4425 separator. Measurements were carried out at 25, 43, 59, 80 and 100 °C. It was found that the equilibrium of ion adsorption-desorption process is shifted towards desorption and faradaic processes occur with the increase in temperature leading to the decrease in capacitance (from 130 to 50 F g^{-1}) and lengthening the relaxation time at elevated temperatures ($T \geq 80$ °C). Therefore, it is not reasonable to suggest RTIL based EDLCs to be used at constantly elevated temperature, as promoted by some authors.

The comparison of RTIL based EDLCtcs with other electrolyte based EDLCtcs studied, it was established that the electrochemical characteristics of EDLCtcs depend strongly on electrolyte composition and electrode structure. It was demonstrated that compatibility of properties of used electrode material, electrolyte and separator is extremely important. The best results amongst RTIL based EDLCtcs where achieved by C(TiC)|$EMImBF_4$ based EDLCtc at 25 °C demonstrating high capacitance (130 F g^{-1}), energy density (47 W h kg^{-1}) and power density (145 kW kg^{-1}) and shortest relaxation time (3.4 s). However, higher power density (270 kW kg^{-1}) and 3 times faster relaxation times (0.5 s) were achieved for more conventional organic solvent electrolyte based EDLCtcs. It has been emphasized, that the high power density and short relaxation time constant of EDLCs are favorable instead of higher energy density because there is a wide selection of batteries with specific energy up to 100 times higher compared to EDLCs studied but lack of high power density devices. Thus, studies made have pointed out that to make RTIL based EDLCs more competitive to organic solvent electrolyte based EDLCs, the following studies in the field of RTIL based EDLCs should focus on lowering the internal resistance of electrode, electrolyte and separator system and increasing the region of electrochemical stability of RTIL based EDLCs.

8. REFERENCES

1. B. E. Conway, Electrochemical Supercapacitors, Scientific Fundamentals and Technological Applications, Kluwer Academic/Plenum: New York, 1999.
2. R. Kötz, M. Carlen, Electrochim. Acta 45 (2000) 2483–2498.
3. A. G. Pandolfo, A. F. Hollenkamp, J. Power Sources 157 (2006) 11–27.
4. P. L. Taberna, P. Simon, J. F. Fauvarque, J. Electrochem. Soc. 150 (2003) A292–A300.
5. F. Beguin, E. Frackowiak, Carbons for Electrochemical Energy Storage and Conversion Systems, CRC Press, New York, 2010.
6. A. Lewandowski, M. Galinski, J. Power Sources 173 (2007) 822–828.
7. M. Arulepp, J. Leis, M. Lätt, F. Miller, K. Rumma, E. Lust, A. F. Burke, J. Power Sources 162 (2006) 1460–1466.
8. H. Kurig, A. Jänes, E. Lust, J. Mater. Res. 25 (2010) 1447–1450.
9. E. Lust, G. Nurk, A. Jänes M. Arulepp, P. Nigu, P. Möller, S. Kallip, V. Sammelselg, J. Solid State Electrochem. 7 (2004) 91–105.
10. L. Permann, M. Lätt, J. Leis, M. Arulepp, Electrochim. Acta 51 (2006) 1274–1281.
11. T. Tsuda, C. L. Hussey, Electrochem. Soc. Interface 1 (2007) 42–49.
12. M. Galinski, A. Lewandowski, I. Stepniak, Electrochim. Acta 51 (2006) 5567–5580.
13. H. Kurig, A. Jänes, E. Lust, J. Electrochem. Soc. 157 (2010) A272–A279.
14. H. Kurig, M. Vestli, A. Jänes, E. Lust, Electrochem. Solid-State Lett. 14 (2011) A120–A122.
15. L. Wei, G. Yushin, J. Power Sources 196 (2011) 4072–4079.
16. A. A. Kornyshev, J. Phys. Chem. B 111 (2007) 5545–5557.
17. R. Lin, P. Huang, J. Segalini, C. Largeot, P. L. Taberna, J. Chmiola, Y. Gogotsi, P. Simon, Electrochim. Acta 54 (2009) 7025–7032.
18. A. Balducci, U. Bardi, S. Caporali, M. Mastragostino, F. Soavi, Electrochem. Commun. 6 (2004) 566–570.
19. A. Lewandowski, M. Galinski, J. Phys. Chem. Solids 65 (2004) 281–286.
20. A. Lewandowski, A. Olejniczak, M. Galinski, I. Stepniak, J. Power Sources 195 (2010) 5814–5819.
21. M. Lazzari, F. Soavi, M. Mastragostino, Fuel Cells 10 (2010) 840–847.
22. C. Arbizzani, M. Biso, D. Cericola, M. Lazzari, F. Soavi, M. Mastragostino, J. Power Sources 185 (2008) 1575–1579.
23. C. Arbizzani, S. Beninati, M. Lazzari, F. Soavi, M. Mastragostino, J. Power Sources 174 (2007) 648–652.
24. M. Lazzari, M. Mastragostino, F. Soavi, Electrochem. Commun. 9 (2007) 1567–1572.
25. A. Balducci, R. Dugas, P. L. Taberna, P. Simon, D. Plee, M. Mastragostino, S. Passerini, J. Power Sources 165 (2007) 922–927.
26. M. Lazzari, M. Mastragostino, A. G. Pandolfo, V. Ruiz, F. Soavi, J. Electrochem. Soc. 158 (2011) A22–A25.
27. J. P. Zheng, P. C. Goonetilleke, C. M. Pettit, D. Roy, Talanta 81 (2010) 1045–1055.
28. J. P. Zheng, C. M. Pettit, P. C. Goonetilleke, C. M. Zenger, D. Roy, Talanta 78 (2009) 1056–1062.
29. L. Siinor, K. Lust, E. Lust, Electrochem. Commun. 12 (2010) 1058–1061.

30. L. Siinor, K. Lust, E. Lust, J. Electrochem. Soc. 157 (2010) F83-F87.
31. S. Zhang, N. Sun, X. He, X. Lu, X. Zhang, J. Phys. Chem. Ref. Data 35 (2006) 1475–1517.
32. J. R. Miller, A. F. Burke, Electrochem. Soc. Interface 1 (2008) 53–57.
33. J. R. Miller, P. Simon, Science 321 (2008) 651–652.
34. P. Simon, A. Burke, Electrochem. Soc. Interface 1 (2008) 38–43.
35. H. Helmholtz, D. Gesetze, Pogg. Ann. LXXXIX (1853) 211.
36. A. Hamelin, T. Vitanov, E. Sevastyanov, A. Popov, J. Electroanal. Chem. Interfacial Electrochem. 145 (1983) 225–264.
37. B. B. Damaskin, O. A. Petrii, V. V. Batrakov, Plenum Press, New York, 1971.
38. L. G. Gouy, J. Phys. IV 9 (1910) 457–468.
39. D. L. Chapman, Philos. Mag. 24 (1913) 475–481.
40. O. Stern, Z. Elektrochem. 30 (1924) 508–511.
41. A. Hamelin, in O'M. Bockris, B. E. Conway ja R. E. White (Eds.) Modern Aspects of Electrochemistry, Vol. 16, Plenum Press, New York, 1985.
42. D. C. Grahame, J. Am. Chem. Soc. 76 (1954) 4819–4823.
43. D. C. Grahame, Z. Electrochem. 59 (1955) 740–743.
44. A. N. Frumkin, Potentsialy Nulevogo Zaryada (Potentials of Zero Charge), Nauka: Moscow (1979) 206.
45. D. C. Grahame, Chem. Rev. 41 (1947) 441–501.
46. J. P. Badiali, M. L. Rosinberg, F. Vericat, L. Blum, J. Electroanal. Chem. Interfacial Electrochem. 158 (1983) 253–267.
47. S. Amokrane, J. P. Badiali, in J. O'M. Bockris, B. E. Conway, R. E. White (Eds.), Modern Aspects of Electrochemsitry, Vol 22, Plenum Press, New York, 1991.
48. Y. Gogotsi (Ed.), Nanomaterials Handbook, CRC Taylor & Francis, Florida, 2006.
49. D. Lozano-Castello, D. Cazorla-Amoros, A. Linares-Solano, S. Shiraishi, H. Kurihara, A. Oya, Carbon 41 (2003) 1765–1775.
50. A. Yoshida, S. Nonaka, I. Aoki, A. Nishino, J. Power Sources 60 (1996) 213–218.
51. S. Brunauer, P. H. Emmett, E. Teller, J. Am. Chem. Soc. 60 (1983) 309–319.
52. S. Urbonaite, S. Wachtmeister, C. Mirguet, E. Coronel, W. Y. Zou, S. Csillag, G. Svensson, Carbon 45 (2007) 2047–2053.
53. T. Thomberg, A. Jänes, E. Lust, J. Electroanal. Chem. 630 (2009) 55–62.
54. E. Frackowiak, K. Jurewicz, K. Szostak, S. Depleux, F. Beguin, Fuel Process. Technol. 77/78 (2002) 213–219.
55. E. Frackowiak, S. Depleux, K. Jurewicz, K. Szostak, D. Cazorla-Amoros, F. Beguin, Chem. Phys. Lett. 361 (2002) 35–41.
56. E. Frackowiak, F. Beguin, Carbon 39 (2001) 937–950.
57. F. Frackowiak, K. Metenier, V. Bertagna, F. Beguin, Appl. Phys. Lett. 77 (2001) 2421–2423.
58. A. V. Kiselev, Y. A. Eltekov, Proceedings of the Second International Congress on Surface Activity, Butterworths, London, 1957.
59. J. H. de Boer, B. C. Lippens, B. G. Lippens, J. C. P. Broekhoff, A. van den Heuvel, T. V. Osinga, J. Colloid Interface Sci. 21 (1966) 405–440.
60. G. D. Halsey, J. Chem. Phys. 16 (1948) 931–937.
61. W. D. Harkins, G. Jura, J. Am. Chem. Soc. 66 (1944) 1362–1366.
62. W. D. Harkins, G. Jura, J. Am. Chem. Soc. 66 (1944) 1366–1373.
63. M. J. G. Janssen, C. W. M. van Oorschot, Proc. 8th IZ Conf., Amsterdam, July 10–14, 1989 Stud. Surf. Sci. Catal. (1989).
64. R. Evans, U. M. B. Marconi, P. Tarazona, J. Chem. Phys. 84 (1986) 2376–2400.

65. K. Tõnurist, A. Jänes, T. Thomberg, E. Lust, J. Electrochem. Soc. 156 (2009) A334–A342.
66. S. S. Zhang, J. Power Sources 164 (2007) 351–364.
67. J. Vila, P. Gines, J. M. Pico, C. Franjo, E. Jimenez, L. M. Varela, O. Cabeza, Fluid Phase Equilib. 242 (2006) 141–146.
68. K. R. Seddon, Nat. Mater. 2 (2003) 363–365.
69. H. Vogel, Phys. Z. 22 (1921) 645–646.
70. G. Tammann, W. Hesse, Z. Anorg, Allg. Chem. 156 (1926) 245–257.
71. G. S. Fulcher, J. Am. Ceram. Soc. 8 (1925) 339–355.
72. H. Ohno (Ed.), Electrochemical Aspects of Ionic Liquids, Wiley-Interscience, New Jersey, 2005.
73. A. Klamt, COSMO-RS: From Quantum Chemistry to Fluid Phase Thermodynamics and Drug Design; Elsevier Science Ltd., Amsterdam, 2005.
74. F. Eckert, A. Klamt, COSMOtherm, Version C2.1, Revision 01.10; COSMOlogic GmbH&CoKG, Leverkusen, 2006.
75. R. Alrichs, M. Bär, H.-P. Baron, R. Bauernschmitt, S. Böcker, M. Ehrig, K. Eichkorn, S. Elliot, F. Furche, F. Haase, M. Häser, H. Horn, C. Hattig, C. Huber, U. Huniar, M. Kattennek, M. Köhn, C. Kölem, M. Kollwitz, K. May, C. Ochsenfeld, H. Öhm, A. Schäfer, U. Schneider, O. Treutler, M. von Arnim, F. Weigend, P. Weis, H. Weiss, Turbomole Version 5.8, 2005.
76. K. Kaupmees, I. Kaljurand, I. Leito, J. Phys. Chem. A 114 (2010) 11788–11793.
77. E. Barsoukov, J. R. Mcdonald, Impedance spectroscopy. Theory, Experiment and Applications, 2nd ed.; Wiley-Interscience, Hoboken, 2005.
78. J. P. Meyers, M. Doyle, R. M. Darling, J. Newman, J. Electrochem. Soc. 147 (2000) 2930–2940.
79. M. Eikerling, A. A. Kornyshev, E. Lust, J. Electrochem. Soc. 152 (2005) E24–E33.
80. F. Scholz (Ed.), Electroanalytical Methods. Guide to Experiments and Applications, Springer, Berlin, 2005.
81. K. S. Cole, R. H. Cole, J. Phys. Chem. 9 (1941) 341–351.
82. D. Qu, H. Shi, J. Power Sources 74 (1998) 99–107.
83. H. K. Song, Y. H. Jung, K. H. Lee, L. H. Dao, Electrochim. Acta 44 (1999) 3513–3519.
84. H. Keiser, K. D. Beccu, M. A. Gutjahr, Electrochim. Acta 21 (1976) 539–543.
85. Y. A. Maletin, N. G. Strizhakova, V. Y. Izotov, A. A. Mironova, S. G. Kozachkov, V. V. Danilin, S. N. Podmogilny, M. Arulepp, J. A. Kukushkina, A. J. Kravchik, V. V. Sokolov, A. Perkson, J. Leis, J. Zheng, S. K. Gordeev, J. Y. Kolotilova, J. Cederström, C. L. Wallace, PCT Patent Application No PCT/WO 02/39468, 2002.
86. S. J. Gregg, K. S. W. Sing, Adsorption, Surface Area and Porosity, Academic, London, 1982.
87. ZView for Windows, Version 3.2; Scribner, Southern Pines, 2010.
88. W. Lorenz, G. Salie, J. Electroanal. Chem. 80 (1977) 1–56.
89. R. Parsons, Advances in Electrochemistry and Electrochemical Engineering 7, Interscience, New York, 1970.
90. B. Damaskin, U. Palm, M. Väärtnõu, J. Electroanal. Chem. 70 (1976) 103–115.
91. U. V. Palm, B. B. Damaskin, Itogi Nauku Tekh., Ser. Elekrokhim. 12 (1977) 99–143.
92. M. Väärtnõu, E. Lust, Electrochim. Acta 45 (2000) 1623–1629.
93. K. Lust, M. Väärtnõu, E. Lust, J. Electroanal. Chem. 532 (2002) 303–316.

94. L. Siinor, K. Lust, E. Lust, J. Electroanal. Chem. 601 (2007) 39–46.
95. A. Jänes, H. Kurig, T. Romann, E. Lust, Electrochem. Commun. 12 (2010) 535–539.
96. B. Scrosati, J. Garche, J. Power Sources 195 (2010) 2419–2430.

9. SUMMARY IN ESTONIAN

"Ioonsetel vedelikel baseeruvad elektrilise kaksikkihi kondensaatorid"

Uuriti toatemperatuuril ioonsete vedelike (TIV) ((1-etüül-3-metüül-imidasooliumtetrafluoroboraat ($EMImBF_4$), 1-etüül-3-metüültetratsüanoboraat ($EMImB(CN)_4$), 1-etüül-3-metüültris(pentafluoroetüül)triluorofosfaat ($EMIm\text{-}PF_3(C_2F_3)_3$), 1-etüül-3-metüülimidasooliumbis(trifluorometüülsulfonüül)imiid ($EMImN(SO_2CF_3)$), 1-etüül-3-metüülbis(fluorosulfonüül)imiid ($EMImN\text{-}(SO_2F)_2$) ja 1-etüül-3-metüülimidasooliumtiotsüanaat (EMImSCN)) sobivust elektrilise kaksikkihi kondensaatori (EKKK) elektrolüüdiks kasutades elektroodidena mikropoorsest süsinikkangast ja tselluloosist separaatorit TF4425. Kõige laiemat ideaalse polariseeritavuse ala (3,2 V) omasid $EMImBF_4$-l ja $EMImB(CN)_4$-l baseeruvad EKKK-d tagades kõrgeima mahtuvuse (~125 F g^{-1}), energia (vastavalt 45 ja 49 W h kg^{-1}) ja võimsustiheduse (vastavalt 36 ja 31 kW kg^{-1}). Näidati, et EKKK-de elektrokeemilised omadused sõltuvad oluliselt ioonsete vedelike koostises oleva aniooni keemilisest koostisest, struktuurist ja aniooni polariseeritavusest ning on tugevalt seotud elektrolüüdi füüsikaliste omadustega nagu juhtivus ja viskoossus.

Temperatuuri mõju TIV-l baseeruvate EKKK-de elektrokeemiliste omaduste uurimiseks koostati $EMImBF_4$, TiC-st sünteesitud süsinikelektroodidest C(TiC) ja TF4425 separaatorist testrakud, mida testiti temperatuuridel 25, 43, 59, 80 ja 100 °C. Leiti, et temperatuuri kasvades ioonide adsorptsiooni-desorptsiooni tasakaal nihkub desorptsiooni suunas ja kahjuks hakkavad toimuma ka Faraday protsessid, tuues kaasa mahtuvuse vähenemise 130 F g^{-1}-lt 50 F g^{-1}-ni ja relaksatsiooniaja kasvamise. Seetõttu ei ole põhjendatud eelistada TIV-l baseeruvate EKKKde kasutamist kõrgematel temperatuuridel, nagu soovitavad mõned autorid.

TIV-l baseeruvate EKKK-de võrdlusest orgaanilistel lahustitel (atsetonitriil, γ-butürolaktoon) ja erinevatel sooladel (trietüülmetüülammoniumtetrafluoroboraat, N,N-dimetüül–1,4-diasabitsüklo[2,2,2]oktaandiiumtetrafluoroboraat, tetrakis(dietüülamino)fosfooniumheksafluorofosfaat) baseeruvate EKKK-dega oli näha, et EKKK-de elektrokeemilised omadused sõltuvad tugevasti elektrolüüdi ja elektroodi keemilisest koostisest, struktuurist ja kokkusobivusest üksteise ja separaatormaterjalidega. Parimaid tulemusi TIV-l baseeruvatest EKKK-dest andsid C(TiC) elektroodidel ja $EMImBF_4$-l baseeruvad EKKK-d, tagades kõrge mahtuvuse (130 F g^{-1}), energia- (47 W h kg^{-1}) ja võimsustiheduse (145 kW kg^{-1}) ning lühima relaksatsiooniaja (3,4 s). Siiski oli orgaanilist solventi sisaldaval elektrolüüdil põhineva EKKK-de võimsustihedus (270 kW kg^{-1}) suurem ja relaksatsiooniaeg lühem (0,5 s) kui parimal TIV-l baseeruval süsteemil. Siinkohal tuleb rõhutada, et kõrge võimsustihedus ja lühike relaksatsiooniaeg on eelistatumad kui kõrge energiatihedus, sest suurema energiatihedusega kuid samas madala võimsustihedusega patareide valik on väga lai. Tehtud uuringud näitasid, et TIV-l baseeruvate EKKK-de konkurentsivõimelisemaks muutmiseks peaksid edasised uuringud keskenduma TIV-l baseeruvate EKKK-de sisetakistuse vähendamisele ja elektrokeemilise stabiilsuse tõstmisele.

10. ACKNOWLEDGEMENTS

First and foremost, I would like to express my greatest gratitude to my supervisors Professor Enn Lust, and Dr. Alar Jänes for their patience, guidance and support through the entire time of collaboration. Also, thanks to Ivo Leito and Karl Kaupmees for guidance on COSMO-RS and Turbomole calculations and allowing me to carry these calculations out at the computer cluster of The Chair of Analytical Chemistry. Many thanks go to Kerli Tõnurist for differential scanning calorimetry measurements, Lauri Jalukse for Karl-Fischer titration measurements and to my other colleagues for encouragement, advice and continuous support.

Last but not least, I would like to thank my family and friends for supporting me all the time.

This research is financially supported by graduate school „Functional materials and processes“ (European Social Fund project 1.2.0401.09–0079), The Estonian Ministry of Education and Research (project SF0180002s08), European Regional Development Fund (projects SLOKT10209T and TAP2-15), Estonian Science Foundation (projects no. 6696, 7606 and 8172), COST actions 542 and MP1004.

11. PUBLICATIONS

CURRICULUM VITAE

General

Name:	Heisi Kurig
Date of birth:	15.06.1985
Citizenship:	Estonian
Address, telephone, e-mail:	Ravila 30–18, 50408 Tartu, Estonia +372 5336 5618, heisi.kurig@ut.ee

Education

Higher education, University of Tartu, Master's degree, 2009. a.

Professional carreer

2009– …	University of Tartu, chemist
2006–2009	University of Tartu, laboratorian

List of publications

1) A. Hallik, A. Alumaa, H. Kurig, A. Jänes, E. Lust, J. Tamm, Synthetic Met. 157 (2007) 1085.
2) A. Jänes, H. Kurig, E. Lust, Carbon 45 (2007) 1226.
3) A. Jänes, H. Kurig, E. Lust, ECS Trans. 3 (2007) 39.
4) G. Nurk, R. Küngas, I. Kivi, H. Kurig, V. Grozovski, S. Kallip, E. Lust, ECS Trans. 7 (2007) 1609.
5) E. Lust, I. Kivi, G. Nurk, P, Möller, S. Kallip, V. Grozovski, H. Kurig, ECS Trans. 7 (2007) 1071.
6) I. Kivi, P. Möller, H. Kurig, S. Kallip, G. Nurk, E. Lust, Electrochem. Commun. 10 (2008) 1455.
7) E. Lust, G. Nurk, I. Kivi, R. Küngas, P. Möller, H. Kurig, S. Kallip, ECS Trans. 12 (2008) 293.
8) A. Jänes, T. Thomberg, K. Tõnurist, H. Kurig, A. Laheäär, E. Lust, ECS Trans. 16 (2008) 57.
9) K. Tõnurist, A. Jänes, T. Thomberg, H. Kurig, E. Lust, J. Electrochem. Soc. 156 (2009) A334.
10) A. Jänes, T. Thomberg, H. Kurig, E. Lust, Carbon 47 (2009) 23.
11) A. Laheäär, H. Kurig, A. Jänes, E. Lust, Electrochim. Acta 54 (2009) 4587.
12) E. Lust, I. Kivi, R. Küngas, K. Tamm, P. Möller, A. Samussenko, E. Anderson, H. Kurig, G. Nurk, ECS Trans. 25 (2009) 325.

35

13) H. Kurig, A. Jänes, E. Lust, J. Electrochem. Soc. 157 (2010) A272.
14) A. Jänes, H. Kurig, T. Romann, E. Lust, Electrochem. Commun. 12 (2010) 535.
15) H. Kurig, A. Jänes, E. Lust, J. Mater. Res. 25 (2010) 1447.
16) E. Lust, R. Küngas, I. Kivi, H. Kurig, P. Möller, E. Anderson, K. Lust, K. Tamm, A. Samussenko, G. Nurk, Electrochim. Acta 55(26) (2010) 7669.
17) H. Kurig, T. Romann, A. Jänes, E. Lust, ECS Trans. 25 (2010) 15.
18) T. Thomberg, H. Kurig, A. Jänes, E. Lust, Microporous Mesoporous Mater. 141(1–3) (2011) 88.
19) H. Kurig, M. Vestli, A. Jänes, E. Lust, Electrochem. Solid-State Lett. 14 (2011) A120
20) A. Jänes, T. Romann, H. Kurig, E. Lust, ECS Trans. 27 (2011) 47.
21) H. Kurig, M Vestli, K. Tõnurist, A. Jänes, E. Lust (under review).

ELULOOKIRJELDUS

Üldandmed

Ees- ja perekonna nimi:	Heisi Kurig
Sünniaeg:	15.06.1985
Kodakondsus:	Eesti
Aadress, telefon, e-mail:	Ravila 30–18, 50408 Tartu, Eesti +372 5336 5618, heisi.kurig@ut.ee

Haridus

Kõrgharidus, Tartu Ülikool, magistrikraad, 2009. a.

Teenistuskäik:

2009– praeguseni	Tartu, Ülikool, keemik
2006–2009	Tartu Ülikool, laborant

Teaduspublikatsioonide loetelu

1) A. Hallik, A. Alumaa, H. Kurig, A. Jänes, E. Lust, J. Tamm, Synthetic Met. 157 (2007) 1085.
2) A. Jänes, H. Kurig, E. Lust, Carbon 45 (2007) 1226.
3) A. Jänes, H. Kurig, E. Lust, ECS Trans. 3 (2007) 39.
4) G. Nurk, R. Küngas, I. Kivi, H. Kurig, V. Grozovski, S. Kallip, E. Lust, ECS Trans. 7 (2007) 1609.
5) E. Lust, I. Kivi, G. Nurk, P, Möller, S. Kallip, V. Grozovski, H. Kurig, ECS Trans. 7 (2007) 1071.
6) I. Kivi, P. Möller, H. Kurig, S. Kallip, G. Nurk, E. Lust, Electrochem. Commun. 10 (2008) 1455.
7) E. Lust, G. Nurk, I. Kivi, R. Küngas, P. Möller, H. Kurig, S. Kallip, ECS Trans. 12 (2008) 293.
8) A. Jänes, T. Thomberg, K. Tõnurist, H. Kurig, A. Laheäär, E. Lust, ECS Trans. 16 (2008) 57.
9) K. Tõnurist, A. Jänes, T. Thomberg, H. Kurig, E. Lust, J. Electrochem. Soc. 156 (2009) A334.
10) A. Jänes, T. Thomberg, H. Kurig, E. Lust, Carbon 47 (2009) 23.
11) A. Laheäär, H. Kurig, A. Jänes, E. Lust, Electrochim. Acta 54 (2009) 4587.
12) E. Lust, I. Kivi, R. Küngas, K. Tamm, P. Möller, A. Samussenko, E. Anderson, H. Kurig, G. Nurk, ECS Trans. 25 (2009) 325.

13) H. Kurig, A. Jänes, E. Lust, J. Electrochem. Soc. 157 (2010) A272.
14) A. Jänes, H. Kurig, T. Romann, E. Lust, Electrochem. Commun. 12 (2010) 535.
15) H. Kurig, A. Jänes, E. Lust, J. Mater. Res. 25 (2010) 1447.
16) E. Lust, R. Küngas, I. Kivi, H. Kurig, P. Möller, E. Anderson, K. Lust, K. Tamm, A. Samussenko, G. Nurk, Electrochim. Acta 55(26) (2010) 7669.
17) H. Kurig, T. Romann, A. Jänes, E. Lust, ECS Trans. 25 (2010) 15.
18) T. Thomberg, H. Kurig, A. Jänes, E. Lust, Microporous Mesoporous Mater. 141(1–3) (2011) 88.
19) H. Kurig, M. Vestli, A. Jänes, E. Lust, Electrochem. Solid-State Lett. 14 (2011) A120.
20) A. Jänes, T. Romann, H. Kurig, E. Lust, ECS Trans. 27 (2011) 47.
21) H. Kurig, M Vestli, K. Tõnurist, A. Jänes, E. Lust (under review).

DISSERTATIONES CHIMICAE UNIVERSITATIS TARTUENSIS

1. **Toomas Tamm.** Quantum-chemical simulation of solvent effects. Tartu, 1993, 110 p.
2. **Peeter Burk.** Theoretical study of gas-phase acid-base equilibria. Tartu, 1994, 96 p.
3. **Victor Lobanov.** Quantitative structure-property relationships in large descriptor spaces. Tartu, 1995, 135 p.
4. **Vahur Mäemets.** The ^{17}O and ^{1}H nuclear magnetic resonance study of H_2O in individual solvents and its charged clusters in aqueous solutions of electrolytes. Tartu, 1997, 140 p.
5. **Andrus Metsala.** Microcanonical rate constant in nonequilibrium distribution of vibrational energy and in restricted intramolecular vibrational energy redistribution on the basis of slater's theory of unimolecular reactions. Tartu, 1997, 150 p.
6. **Uko Maran.** Quantum-mechanical study of potential energy surfaces in different environments. Tartu, 1997, 137 p.
7. **Alar Jänes.** Adsorption of organic compounds on antimony, bismuth and cadmium electrodes. Tartu, 1998, 219 p.
8. **Kaido Tammeveski.** Oxygen electroreduction on thin platinum films and the electrochemical detection of superoxide anion. Tartu, 1998, 139 p.
9. **Ivo Leito.** Studies of Brønsted acid-base equilibria in water and non-aqueous media. Tartu, 1998, 101 p.
10. **Jaan Leis.** Conformational dynamics and equilibria in amides. Tartu, 1998, 131 p.
11. **Toonika Rinken.** The modelling of amperometric biosensors based on oxidoreductases. Tartu, 2000, 108 p.
12. **Dmitri Panov.** Partially solvated Grignard reagents. Tartu, 2000, 64 p.
13. **Kaja Orupõld.** Treatment and analysis of phenolic wastewater with microorganisms. Tartu, 2000, 123 p.
14. **Jüri Ivask.** Ion Chromatographic determination of major anions and cations in polar ice core. Tartu, 2000, 85 p.
15. **Lauri Vares.** Stereoselective Synthesis of Tetrahydrofuran and Tetrahydropyran Derivatives by Use of Asymmetric Horner-Wadsworth-Emmons and Ring Closure Reactions. Tartu, 2000, 184 p.
16. **Martin Lepiku.** Kinetic aspects of dopamine D_2 receptor interactions with specific ligands. Tartu, 2000, 81 p.
17. **Katrin Sak.** Some aspects of ligand specificity of P2Y receptors. Tartu, 2000, 106 p.
18. **Vello Pällin.** The role of solvation in the formation of iotsitch complexes. Tartu, 2001, 95 p.

19. **Katrin Kollist.** Interactions between polycyclic aromatic compounds and humic substances. Tartu, 2001, 93 p.
20. **Ivar Koppel.** Quantum chemical study of acidity of strong and superstrong Brønsted acids. Tartu, 2001, 104 p.
21. **Viljar Pihl.** The study of the substituent and solvent effects on the acidity of OH and CH acids. Tartu, 2001, 132 p.
22. **Natalia Palm.** Specification of the minimum, sufficient and significant set of descriptors for general description of solvent effects. Tartu, 2001, 134 p.
23. **Sulev Sild.** QSPR/QSAR approaches for complex molecular systems. Tartu, 2001, 134 p.
24. **Ruslan Petrukhin.** Industrial applications of the quantitative structure-property relationships. Tartu, 2001, 162 p.
25. **Boris V. Rogovoy.** Synthesis of (benzotriazolyl)carboximidamides and their application in relations with *N*- and *S*-nucleophyles. Tartu, 2002, 84 p.
26. **Koit Herodes.** Solvent effects on UV-vis absorption spectra of some solvatochromic substances in binary solvent mixtures: the preferential solvation model. Tartu, 2002, 102 p.
27. **Anti Perkson.** Synthesis and characterisation of nanostructured carbon. Tartu, 2002, 152 p.
28. **Ivari Kaljurand.** Self-consistent acidity scales of neutral and cationic Brønsted acids in acetonitrile and tetrahydrofuran. Tartu, 2003, 108 p.
29. **Karmen Lust.** Adsorption of anions on bismuth single crystal electrodes. Tartu, 2003, 128 p.
30. **Mare Piirsalu.** Substituent, temperature and solvent effects on the alkaline hydrolysis of substituted phenyl and alkyl esters of benzoic acid. Tartu, 2003, 156 p.
31. **Meeri Sassian.** Reactions of partially solvated Grignard reagents. Tartu, 2003, 78 p.
32. **Tarmo Tamm.** Quantum chemical modelling of polypyrrole. Tartu, 2003. 100 p.
33. **Erik Teinemaa.** The environmental fate of the particulate matter and organic pollutants from an oil shale power plant. Tartu, 2003. 102 p.
34. **Jaana Tammiku-Taul.** Quantum chemical study of the properties of Grignard reagents. Tartu, 2003. 120 p.
35. **Andre Lomaka.** Biomedical applications of predictive computational chemistry. Tartu, 2003. 132 p.
36. **Kostyantyn Kirichenko.** Benzotriazole – Mediated Carbon–Carbon Bond Formation. Tartu, 2003. 132 p.
37. **Gunnar Nurk.** Adsorption kinetics of some organic compounds on bismuth single crystal electrodes. Tartu, 2003, 170 p.
38. **Mati Arulepp.** Electrochemical characteristics of porous carbon materials and electrical double layer capacitors. Tartu, 2003, 196 p.

39. **Dan Cornel Fara.** QSPR modeling of complexation and distribution of organic compounds. Tartu, 2004, 126 p.
40. **Riina Mahlapuu.** Signalling of galanin and amyloid precursor protein through adenylate cyclase. Tartu, 2004, 124 p.
41. **Mihkel Kerikmäe.** Some luminescent materials for dosimetric applications and physical research. Tartu, 2004, 143 p.
42. **Jaanus Kruusma.** Determination of some important trace metal ions in human blood. Tartu, 2004, 115 p.
43. **Urmas Johanson.** Investigations of the electrochemical properties of polypyrrole modified electrodes. Tartu, 2004, 91 p.
44. **Kaido Sillar.** Computational study of the acid sites in zeolite ZSM-5. Tartu, 2004, 80 p.
45. **Aldo Oras.** Kinetic aspects of dATPαS interaction with $P2Y_1$ receptor. Tartu, 2004, 75 p.
46. **Erik Mölder.** Measurement of the oxygen mass transfer through the air-water interface. Tartu, 2005, 73 p.
47. **Thomas Thomberg.** The kinetics of electroreduction of peroxodisulfate anion on cadmium (0001) single crystal electrode. Tartu, 2005, 95 p.
48. **Olavi Loog.** Aspects of condensations of carbonyl compounds and their imine analogues. Tartu, 2005, 83 p.
49. **Siim Salmar.** Effect of ultrasound on ester hydrolysis in aqueous ethanol. Tartu, 2006, 73 p.
50. **Ain Uustare.** Modulation of signal transduction of heptahelical receptors by other receptors and G proteins. Tartu, 2006, 121 p.
51. **Sergei Yurchenko.** Determination of some carcinogenic contaminants in food. Tartu, 2006, 143 p.
52. **Kaido Tämm.** QSPR modeling of some properties of organic compounds. Tartu, 2006, 67 p.
53. **Olga Tšubrik.** New methods in the synthesis of multisubstituted hydrazines. Tartu. 2006, 183 p.
54. **Lilli Sooväli.** Spectrophotometric measurements and their uncertainty in chemical analysis and dissociation constant measurements. Tartu, 2006, 125 p.
55. **Eve Koort.** Uncertainty estimation of potentiometrically measured ph and pK_a values. Tartu, 2006, 139 p.
56. **Sergei Kopanchuk.** Regulation of ligand binding to melanocortin receptor subtypes. Tartu, 2006, 119 p.
57. **Silvar Kallip.** Surface structure of some bismuth and antimony single crystal electrodes. Tartu, 2006, 107 p.
58. **Kristjan Saal.** Surface silanization and its application in biomolecule coupling. Tartu, 2006, 77 p.
59. **Tanel Tätte.** High viscosity $Sn(OBu)_4$ oligomeric concentrates and their applications in technology. Tartu, 2006, 91 p.

60. **Dimitar Atanasov Dobchev**. Robust QSAR methods for the prediction of properties from molecular structure. Tartu, 2006, 118 p.
61. **Hannes Hagu**. Impact of ultrasound on hydrophobic interactions in solutions. Tartu, 2007, 81 p.
62. **Rutha Jäger.** Electroreduction of peroxodisulfate anion on bismuth electrodes. Tartu, 2007, 142 p.
63. **Kaido Viht.** Immobilizable bisubstrate-analogue inhibitors of basophilic protein kinases: development and application in biosensors. Tartu, 2007, 88 p.
64. **Eva-Ingrid Rõõm.** Acid-base equilibria in nonpolar media. Tartu, 2007, 156 p.
65. **Sven Tamp.** DFT study of the cesium cation containing complexes relevant to the cesium cation binding by the humic acids. Tartu, 2007, 102 p.
66. **Jaak Nerut.** Electroreduction of hexacyanoferrate(III) anion on Cadmium (0001) single crystal electrode. Tartu, 2007, 180 p.
67. **Lauri Jalukse.** Measurement uncertainty estimation in amperometric dissolved oxygen concentration measurement. Tartu, 2007, 112 p.
68. **Aime Lust.** Charge state of dopants and ordered clusters formation in CaF_2:Mn and CaF_2:Eu luminophors. Tartu, 2007, 100 p.
69. **Iiris Kahn**. Quantitative Structure-Activity Relationships of environmentally relevant properties. Tartu, 2007, 98 p.
70. **Mari Reinik.** Nitrates, nitrites, N-nitrosamines and polycyclic aromatic hydrocarbons in food: analytical methods, occurrence and dietary intake. Tartu, 2007, 172 p.
71. **Heili Kasuk.** Thermodynamic parameters and adsorption kinetics of organic compounds forming the compact adsorption layer at Bi single crystal electrodes. Tartu, 2007, 212 p.
72. **Erki Enkvist.** Synthesis of adenosine-peptide conjugates for biological applications. Tartu, 2007, 114 p.
73. **Svetoslav Hristov Slavov**. Biomedical applications of the QSAR approach. Tartu, 2007, 146 p.
74. **Eneli Härk.** Electroreduction of complex cations on electrochemically polished Bi(*hkl*) single crystal electrodes. Tartu, 2008, 158 p.
75. **Priit Möller.** Electrochemical characteristics of some cathodes for medium temperature solid oxide fuel cells, synthesized by solid state reaction technique. Tartu, 2008, 90 p.
76. **Signe Viggor.** Impact of biochemical parameters of genetically different pseudomonads at the degradation of phenolic compounds. Tartu, 2008, 122 p.
77. **Ave Sarapuu.** Electrochemical reduction of oxygen on quinone-modified carbon electrodes and on thin films of platinum and gold. Tartu, 2008, 134 p.
78. **Agnes Kütt.** Studies of acid-base equilibria in non-aqueous media. Tartu, 2008, 198 p.

79. **Rouvim Kadis.** Evaluation of measurement uncertainty in analytical chemistry: related concepts and some points of misinterpretation. Tartu, 2008, 118 p.
80. **Valter Reedo.** Elaboration of IVB group metal oxide structures and their possible applications. Tartu, 2008, 98 p.
81. **Aleksei Kuznetsov.** Allosteric effects in reactions catalyzed by the cAMP-dependent protein kinase catalytic subunit. Tartu, 2009, 133 p.
82. **Aleksei Bredihhin.** Use of mono- and polyanions in the synthesis of multisubstituted hydrazine derivatives. Tartu, 2009, 105 p.
83. **Anu Ploom.** Quantitative structure-reactivity analysis in organosilicon chemistry. Tartu, 2009, 99 p.
84. **Argo Vonk.** Determination of adenosine A_{2A}- and dopamine D_1 receptor-specific modulation of adenylate cyclase activity in rat striatum. Tartu, 2009, 129 p.
85. **Indrek Kivi.** Synthesis and electrochemical characterization of porous cathode materials for intermediate temperature solid oxide fuel cells. Tartu, 2009, 177 p.
86. **Jaanus Eskusson.** Synthesis and characterisation of diamond-like carbon thin films prepared by pulsed laser deposition method. Tartu, 2009, 117 p.
87. **Marko Lätt.** Carbide derived microporous carbon and electrical double layer capacitors. Tartu, 2009, 107 p.
88. **Vladimir Stepanov.** Slow conformational changes in dopamine transporter interaction with its ligands. Tartu, 2009, 103 p.
89. **Aleksander Trummal.** Computational Study of Structural and Solvent Effects on Acidities of Some Brønsted Acids. Tartu, 2009, 103 p.
90. **Eerold Vellemäe.** Applications of mischmetal in organic synthesis. Tartu, 2009, 93 p.
91. **Sven Parkel.** Ligand binding to 5-HT_{1A} receptors and its regulation by Mg^{2+} and Mn^{2+}. Tartu, 2010, 99 p.
92. **Signe Vahur.** Expanding the possibilities of ATR-FT-IR spectroscopy in determination of inorganic pigments. Tartu, 2010, 184 p.
93. **Tavo Romann**. Preparation and surface modification of bismuth thin film, porous, and microelectrodes. Tartu, 2010, 155 p.
94. **Nadežda Aleksejeva.** Electrocatalytic reduction of oxygen on carbon nanotube-based nanocomposite materials. Tartu, 2010, 147 p.
95. **Marko Kullapere.** Electrochemical properties of glassy carbon, nickel and gold electrodes modified with aryl groups. Tartu, 2010, 233 p.
96. **Liis Siinor.** Adsorption kinetics of ions at Bi single crystal planes from aqueous electrolyte solutions and room-temperature ionic liquids. Tartu, 2010, 101 p.
97. **Angela Vaasa.** Development of fluorescence-based kinetic and binding assays for characterization of protein kinases and their inhibitors. Tartu 2010, 101 p.

98. **Indrek Tulp.** Multivariate analysis of chemical and biological properties. Tartu 2010, 105 p.
99. **Aare Selberg.** Evaluation of environmental quality in Northern Estonia by the analysis of leachate. Tartu 2010, 117 p.
100. **Darja Lavõgina.** Development of protein kinase inhibitors based on adenosine analogue-oligoarginine conjugates. Tartu 2010, 248 p.
101. **Laura Herm.** Biochemistry of dopamine D_2 receptors and its association with motivated behaviour. Tartu 2010, 156 p.
102. **Terje Raudsepp.** Influence of dopant anions on the electrochemical properties of polypyrrole films. Tartu 2010, 112 p.
103. **Margus Marandi.** Electroformation of Polypyrrole Films: *In-situ* AFM and STM Study. Tartu 2011, 116 p.
104. **Kairi Kivirand.** Diamine oxidase-based biosensors: construction and working principles. Tartu, 2011, 140 p.
105. **Anneli Kruve.** Matrix effects in liquid-chromatography electrospray mass-spectrometry. Tartu, 2011, 156 p.
106. **Gary Urb.** Assessment of environmental impact of oil shale fly ash from PF and CFB combustion. Tartu, 2011, 108 p.
107. **Nikita Oskolkov.** A novel strategy for peptide-mediated cellular delivery and induction of endosomal escape. Tartu, 2011, 106 p.
108. **Dana Martin.** The QSPR/QSAR approach for the prediction of properties of fullerene derivatives. Tartu, 2011, 98 p.
109. **Säde Viirlaid.** Novel glutathione analogues and their antioxidant activity. Tartu, 2011, 106 p.
110. **Ülis Sõukand.** Simultaneous adsorption of Cd^{2+}, Ni^{2+}, and Pb^{2+} on peat. Tartu, 2011, 124 p.
111. **Lauri Lipping.** The acidity of strong and superstrong Brønsted acids, an outreach for the "limits of growth": a quantum chemical study. Tartu, 2011, 124 p.